



# Source and sectoral contribution analysis of PM<sub>2.5</sub> based on efficient response surface modeling technique over Pearl River Delta Region of China

Yuzhou Pan<sup>a</sup>, Yun Zhu<sup>a,\*</sup>, Jicheng Jang<sup>a</sup>, Shuxiao Wang<sup>b</sup>, Jia Xing<sup>b</sup>, Pen-Chi Chiang<sup>c,d</sup>, Xuetao Zhao<sup>e</sup>, Zhiqiang You<sup>a</sup>, Yingzhi Yuan<sup>a</sup>

<sup>a</sup> Guangdong Provincial Key Laboratory of Atmospheric Environment and Pollution Control, School of Environment and Energy, South China University of Technology, Guangzhou Higher Education Mega Center, Guangzhou 510006, China

<sup>b</sup> State Key Joint Laboratory of Environment Simulation and Pollution Control, School of Environment, Tsinghua University, Beijing 100084, China

<sup>c</sup> Graduate Institute of Environmental Engineering, National Taiwan University, Taipei 10673, Taiwan

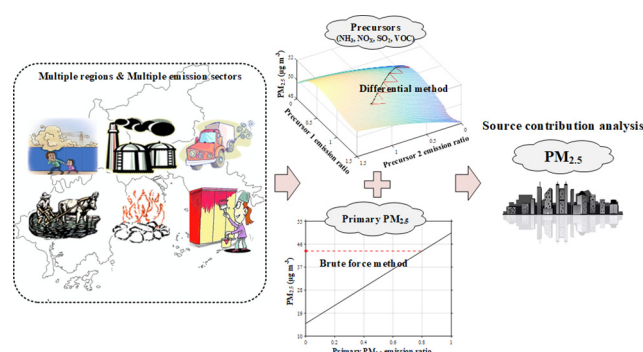
<sup>d</sup> Carbon Cycle Research Center, National Taiwan University, 10672, Taiwan

<sup>e</sup> Chinese Academy of Environmental Planning, Beijing 100012, China

## HIGHLIGHTS

- A response surface modeling technique with differential method (RSM-DM) was developed.
- RSM-DM well resolved the nonlinear quantification issue of brute force method.
- RSM-DM can reproduce accumulative contribution of precursor emissions to PM<sub>2.5</sub>.
- This innovative method was applied to investigate PM<sub>2.5</sub> source contributions in PRD.

## GRAPHICAL ABSTRACT



## ARTICLE INFO

### Article history:

Received 3 January 2020

Received in revised form 20 May 2020

Accepted 22 May 2020

Available online 26 May 2020

Editor: Jianmin Chen

### Keywords:

PM<sub>2.5</sub>  
Response surface model  
Differential method  
Brute force method  
Source contribution

## ABSTRACT

Identifying and quantifying source contributions of pollutant emissions are crucial for an effective control strategy to break through the bottleneck in reducing ambient PM<sub>2.5</sub> levels over the Pearl River Delta (PRD) region of China. In this study, an innovative response surface modeling technique with differential method (RSM-DM) has been developed and applied to investigate the PM<sub>2.5</sub> contributions from multiple regions, sectors, and pollutants over the PRD region in 2015. The new differential method, with the ability to reproduce the nonlinear response surface of PM<sub>2.5</sub> to precursor emissions by dissecting the emission changes into a series of small intervals, has shown to overcome the issue of the traditional brute force method in overestimating the accumulative contribution of precursor emissions to PM<sub>2.5</sub>. The results of this case study showed that PM<sub>2.5</sub> in the PRD region was generally dominated by local emission sources (39–64%). Among the contributions of PM<sub>2.5</sub> from various sectors and pollutants, the primary PM<sub>2.5</sub> emissions from fugitive dust source contributed most (25–42%) to PM<sub>2.5</sub> levels. The contributions of agriculture NH<sub>3</sub> emissions (6–13%) could also play a significant role compared to other sectoral precursor emissions. Among the NO<sub>x</sub> sectors, the emissions control of stationary combustion source could be most effective in reducing PM<sub>2.5</sub> levels over the PRD region.

© 2020 Elsevier B.V. All rights reserved.

\* Corresponding author.

E-mail address: [zhuyun@scut.edu.cn](mailto:zhuyun@scut.edu.cn) (Y. Zhu).

## 1. Introduction

Over the past decade, fine particulate matter or PM<sub>2.5</sub>, has drawn substantial attention in China. The Pearl River Delta (PRD) region has taken the lead in PM<sub>2.5</sub> control over China in recent years. The annual mean PM<sub>2.5</sub> concentration has reached the second-level limit of the National Ambient Air Quality Standards (NAAQS) of China (35 µg m<sup>-3</sup>) consistently from 2015 to 2018 (GDEEP, 2016; GDEEP, 2017; GDEEP, 2018; GDEEP, 2019) but it has now met a bottleneck for the trend of continuous decline. The effective and focused control strategies are urgently needed to further reduce PM<sub>2.5</sub> concentration over the PRD region. PM<sub>2.5</sub> is a complex mixture of the primary compositions directly emitted from various sources together with the secondary components converted from gaseous precursors, which are produced from both local emissions and regional transport. Therefore, identifying and quantifying the emission contributions of multiple pollutants from multiple regions and sectors to PM<sub>2.5</sub> are the preconditions for an effective PM<sub>2.5</sub> control strategy over the PRD region.

Currently, PM<sub>2.5</sub> source contribution analysis or apportionment methods mainly include receptor models and photochemical air quality model-based techniques (Wang et al., 2016a; Xie et al., 2016), as summarized in Table S1 with their strengths and limitations. Receptor models, based on measurement from ambient air by the receptor, e.g., Positive Matrix Factorization (PMF) (Paatero and Tapper, 1994) and Chemical Mass Balance (CMB) (Watson et al., 1984), have been broadly applied mainly because of their simplicity (Bi et al., 2011; Wang et al., 2009). However, receptor models are not capable of distinguishing the contributions from local and regional transportation between or beyond the on-site measurement networks; and this methodology is difficult to identify sources of secondary components (Li et al., 2018). On the other hand, photochemical air quality models are powerful in simulating air quality in different spatial and temporal scales and providing source-receptor relationships for secondary species (Chen et al., 2018; Zhang et al., 2017). There are a number of PM<sub>2.5</sub> source apportionment techniques developed based on photochemical air quality models. One category is the sensitivity analysis, e.g., brute force method (BFM) and decoupled direct method (DDM) (Dunker, 1984; Ivey et al., 2015; Koo et al., 2009). However, the nonlinear impact of emission sources on PM<sub>2.5</sub> cannot be quantified properly by BFM; and the DDM is difficult to capture the nonlinearity under large emission perturbations. A higher-order DDM (HDDM) (Hakami et al., 2003) was developed sequentially to handle the nonlinearity. Nevertheless, the HDDM is not reliable for predicting the concentration response to simultaneous emission changes of multiple (>3) variables (Dunker et al., 2002; Hakami et al., 2004). Another category is the tagged tracer technique, e.g., the Particulate Source Apportionment Technology (PSAT) embedded in the Comprehensive Air Quality Model with Extensions (CAMx) (Kim et al., 2017; Li et al., 2015; Wang et al., 2017b; Wen et al., 2016) and the Integrated Source Apportionment Model (ISAM) in the Community Multi-scale Air Quality model (CMAQ) (Chang et al., 2019; Chen et al., 2017; Napelenok et al., 2014). Although the results of tagged tracer technique are reliable due to the full tracking of the reaction process, the use of photochemical air quality models will be resource-intensive and often cannot meet the requirement of time and cost constraints for supporting policy analysis (Xing et al., 2011). To overcome the issue, a series of efficient concentration response methodologies, starting with the response surface model (RSM) (Wang et al., 2011; Xing et al., 2011), extended RSM (ERSM) (Xing et al., 2017; Zhao et al., 2015; Zhao et al., 2017) and RSM/ERSM with polynomial functions (pf-RSM/pf-ERSM) (Xing et al., 2018) have been developed. RSM is a reduced-form prediction model, which builds the relationship between photochemical air quality model outputs and emission inputs using advanced mathematical algorithms. In RSM, the pollutant concentration can respond dynamically to multiple variables under a wide range of emissions perturbation in a real-time manner with the nonlinear characteristics well captured. Therefore, the analyses

of source contributions can be provided by RSM with BFM in unlimited control scenarios in a near real-time manner (You et al., 2017). However, the accumulative contribution of each source reduction provided by BFM will generally be higher than the response to all sources reduction due to the nonlinear relationship between PM<sub>2.5</sub> and precursor emissions (Burr and Zhang, 2011).

Aimed at addressing aforementioned issues, an innovative pf-ERSM with differential method (DM), with the ability to reproduce the nonlinear response surface of PM<sub>2.5</sub> to precursor emissions by dissecting the emission changes into a series of small intervals, was developed to improve the accuracy for source contribution analysis of precursor emissions to PM<sub>2.5</sub>. Meanwhile, the following additional two tasks were carried out in this study: (1) a sectoral linearity (SL) technique, implying the linear relationship between total emissions (i.e., the sum of sectoral emissions) of precursors and sectoral ones, was coupled in pf-ERSM (referred to as "pf-ERSM-SL" hereafter) to further investigate the contributions of precursor emissions from multiple sectors; (2) the RSM with BFM was kept to conduct source contribution analysis of primary PM<sub>2.5</sub> emissions to PM<sub>2.5</sub> (Long et al., 2016). Finally, the pf-ERSM-SL with DM and BFM was applied to quantify the PM<sub>2.5</sub> contributions from multiple regions, sectors, and pollutants over the PRD region in 2015.

## 2. Methodology

Fig. 1 schematically showed the operation process of PM<sub>2.5</sub> source contribution analysis based on pf-ERSM-SL with DM and BFM in the PRD region. Firstly, control factors were selected referring to control policy objectives, and then three control matrices consisting of three sets of emissions control scenarios parameterized by control factors were designed. Secondly, an integrated modeling system combining WRF version 3.9.1 and CMAQ version 5.2 (WRF-CMAQ) was used to conduct air quality simulations under the three kinds of control scenarios for the PRD region in 2015. Thirdly, the pf-ERSM-SL including three relationships was developed based on the simulation results by WRF-CMAQ. Then validation was done to examine the performance of pf-ERSM-SL. Finally, DM and BFM were used to analyze the emission contributions of precursor and primary PM<sub>2.5</sub> from multiple regions and multiple sectors to the PM<sub>2.5</sub> concentrations predicted by pf-ERSM-SL in receptors, respectively. Further details of the process were provided below and in the Supplementary Material.

### 2.1. WRF-CMAQ configuration

Three nested domains denoted as d01, d02, and d03 (Fig. 2a) were used for the WRF-CMAQ simulation system. The outermost domain (d01) with grid resolutions of 27 km × 27 km covered most of China and some other parts of Asia. The middle domain (d02) with grid resolutions of 9 km × 9 km aimed to cover southeastern China, including Guangdong province. The innermost domain (d03) covering the whole PRD region with grid resolutions of 3 km × 3 km was the focus of this study (Fig. 2b). Vertically, twenty sigma layers from the surface to the tropopause were set for all domains.

The WRF model provided the meteorological input data files for the CMAQ model. The NCEP FNL (Final) Operational Global Analysis data (downloaded from <http://dss.ucar.edu/datasets/ds083.2/>) were used to drive the WRF model. Output files of the WRF model were post-processed for the CMAQ model using Meteorology Chemistry Interface Processor (MCIP) program. The Carbon Bond Mechanism (CB6) with aqueous and aerosol extensions was chosen for the gas-phase chemistry module and the AREO5 aerosol mechanism was selected for the aerosol module in the CMAQ model. The initial and boundary conditions for the CMAQ simulation on d01 were generated from default profiles in the CMAQ model while that for d02 and d03 were generated from simulation results on d01 and d02, respectively. A 5-day spin-up period was used to reduce the influence of initial conditions on modeling results.

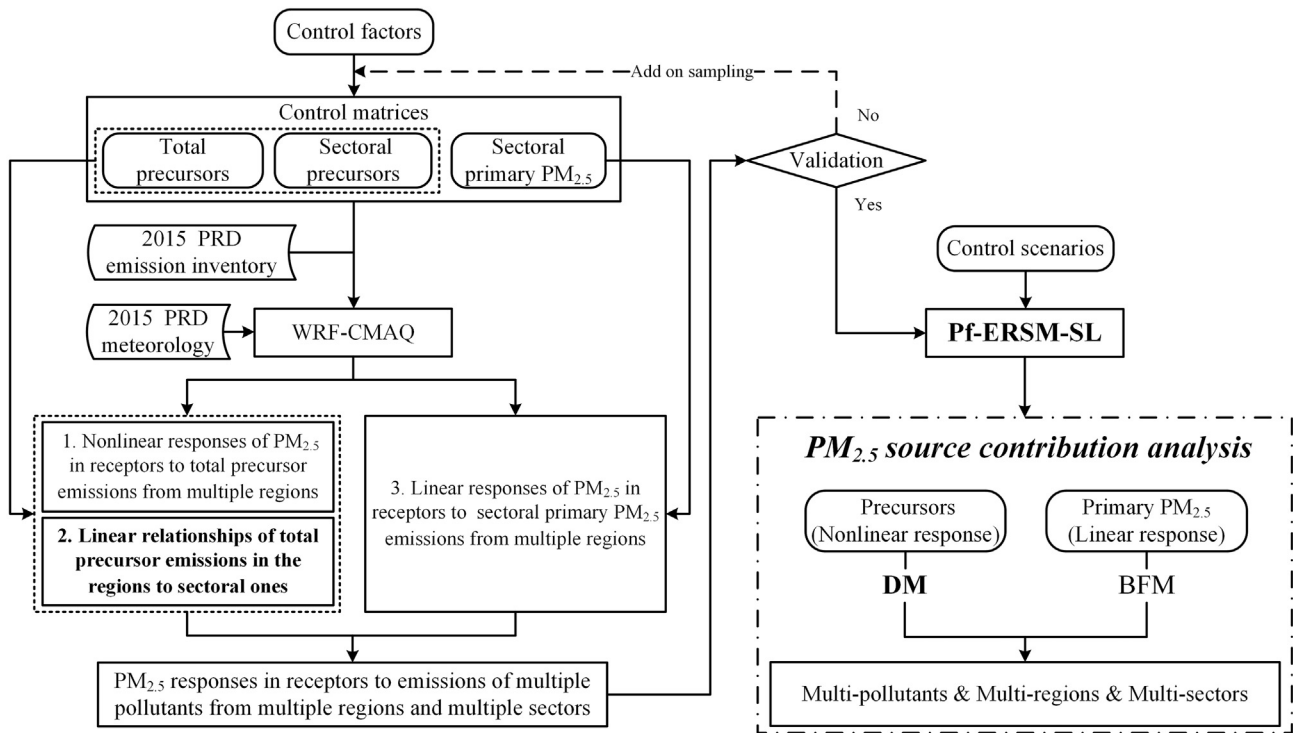


Fig. 1. The operation process of PM<sub>2.5</sub> source contribution analysis based on pf-ERSM-SL with DM and BFM in the PRD region.

The anthropogenic emission inventories for the outer and middle domains were provided by Tsinghua University (Ma et al., 2017). The emission inventory of the innermost domain was from 2015-based emission inventory in Guangdong province, which was developed by the joint research team of Tsinghua University and South China University of Technology. The biogenic emissions were calculated by the Model of Emissions of Gases and Aerosols from Nature (MEGAN) (Guenther et al., 2006).

The innermost simulation area was divided into 7 regions (Fig. 2b), including Shunde (A, SD), Foshan (B, FS), Guangzhou (C, GZ), Zhongshan (D, ZS), Jiangmen (E, JM), Dongguan and Shenzhen (F, DG&SZ), and other regions (G, OTH). The local national-controlled air-monitoring sites in each of 6 regions (except OTH) were chosen to represent the whole of the region for source contribution analysis. The simulation periods were January, April, July, and October in 2015, representing winter, spring, summer, and fall.

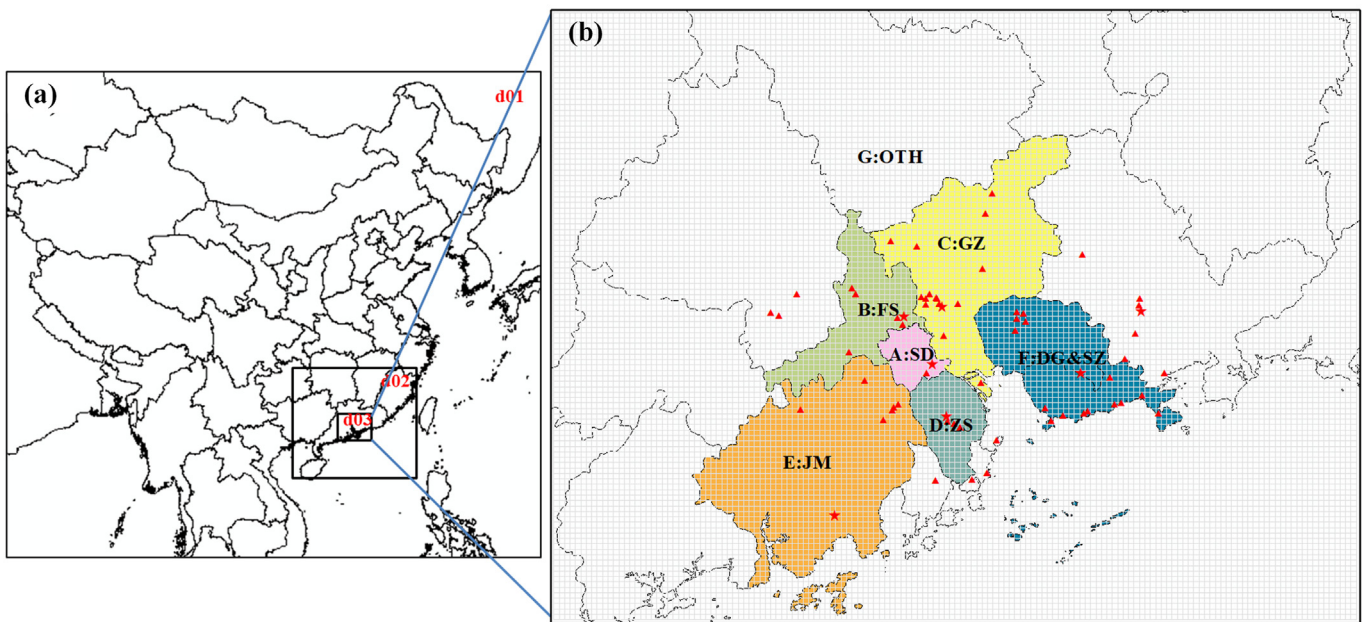


Fig. 2. (a) The three nested domains with 27 km, 9 km, and 3 km used in WRF-CMAQ simulation; (b) The definition of seven regions in the innermost domain, denoted by different colors. The red marks are the locations of the observation sites, among which the ones marked by pentagams were chosen to evaluate PM<sub>2.5</sub> simulation. (For interpretation of the references to colour in this figure legend, the reader is referred to the web version of this article.)

## 2.2. Pf-ERSM-SL development

The pf-ERSM-SL using the pf-ERSM coupled with the SL technique to build the response of PM<sub>2.5</sub> to precursor emissions from multiple regions and sectors. The mathematical fitting process of pf-ERSM-SL was shown in Fig. S1. The pf-ERSM in this study referred to the modified one which was proved to have a better performance by our research team. The detailed methodology had been described in another paper (Fang et al., 2020). In this Sect., some key components of the modified pf-ERSM were given synoptically, and then the SL technique was introduced in detail.

The effects of total emissions of precursors (referred to as “total precursor emissions” hereafter) from multiple regions on PM<sub>2.5</sub> concentrations in receptors in the modified pf-ERSM are from two pathways. One is sum of the single effect of total precursor emissions from every single region (denoted as “SR”). Another is the inter-regional effects among multiple regions (denoted as “IR”). Suppose the receptor region is *A* and the source region is *r* (*r* = *A*, ..., *G*). The response of PM<sub>2.5</sub> concentration at receptor *A* can be represented as follows:

$$\Delta\text{Conc}[\text{PM}_{2.5}]_A = \sum_{r=A, \dots, G} (\Delta\text{Conc}[\text{PM}_{2.5}]_{r \rightarrow A}^{\text{SR}}) + \Delta\text{Conc}[\text{PM}_{2.5}]_A^{\text{IR}} \quad (1)$$

where  $\Delta\text{Conc}[\text{PM}_{2.5}]_A$  is the changes of PM<sub>2.5</sub> concentration compared with the base case at receptor *A*.  $\Delta\text{Conc}[\text{PM}_{2.5}]_{r \rightarrow A}^{\text{SR}}$  and  $\Delta\text{Conc}[\text{PM}_{2.5}]_A^{\text{IR}}$  represent the changes of PM<sub>2.5</sub> concentration at receptor *A* caused by SR and IR, respectively.

SR and IR were quantified by a series of polynomial functions, expressed as Eq. (2). The polynomial functions were fitted by a set of randomly generated emissions control scenarios (Table S2).

$$\Delta\text{Conc}[\text{PM}_{2.5}] = \sum_{i=1}^j X_i \cdot (E[\text{NO}_x])^{a_i} \cdot (E[\text{NH}_3])^{b_i} \cdot (E[\text{SO}_2])^{c_i} \cdot (E[\text{VOC}])^{d_i} \quad (2)$$

where  $\Delta\text{Conc}[\text{PM}_{2.5}]$  is the changes of PM<sub>2.5</sub> concentration.  $E[\text{NO}_x]$ ,  $E[\text{NH}_3]$ ,  $E[\text{SO}_2]$ ,  $E[\text{VOC}]$  are the change ratios of total NO<sub>x</sub>, SO<sub>2</sub>, NH<sub>3</sub>, and VOC emissions related to the baseline (i.e., baseline = 0), respectively;  $a_i$ ,  $b_i$ ,  $c_i$ , and  $d_i$  represent the nonnegative integer powers of  $E[\text{NO}_x]$ ,  $E[\text{NH}_3]$ ,  $E[\text{SO}_2]$  and  $E[\text{VOC}]$ , respectively;  $X_i$  is the coefficient of the term  $i$ .

The pf-ERSM only focused on the precursor emissions without sectoral classification. However, it is necessary to adopt different emissions reduction ratios for sub-sectors according to the actual situation in policy-making. To obtain the real-time response of PM<sub>2.5</sub> to sectoral emissions of precursors (referred to as “sectoral precursor emissions” hereafter), it is crucial to establish the relationship between total precursor emissions and sectoral ones in the presence of the relationship between PM<sub>2.5</sub> response and total precursor emissions.

Considering the main emission sectors of precursors and the different impacts of sectoral precursor emissions on PM<sub>2.5</sub>, NH<sub>3</sub> emission sources were grouped into 2 sectors, i.e., agriculture and other sources (stationary combustion, industrial process, on-road mobile, residential); NO<sub>x</sub> emission sources were classified into 3 sectors, i.e., stationary combustion, on-road mobile, and other sources (industrial process, non-road mobile, agriculture); SO<sub>2</sub> emission sources were classified into 2 sectors, i.e., stationary combustion and other sources (industrial process, on-road mobile, non-road mobile, agriculture), VOC remained total (stationary combustion, industrial process, on-road mobile, non-road mobile, solvent use, fuel oil storage, agriculture and residential). Then there were 7 sectoral control variables of precursors in a single region. The total emissions of one precursor is equal to the sum of emissions from each sector. That is to say, there is an apparent linear relationship between the total precursor emissions and sectoral ones. Therefore 2, 3, and 2 training samples are needed at least for NH<sub>3</sub>, NO<sub>x</sub>, and SO<sub>2</sub> respectively to fit the linear function. Here we adopted the fixed value sample, i.e., sectoral variables of one precursor are set to 0 in turn and the others stay constant, to obtain the training samples. Also, another one case where all sectoral variables of one precursor are set to 0 and the others stay constant was added to improve the fitting accuracy. Then there were 10 training samples in a single region. The control variables setting and the number of scenarios were shown in Table 1.

Different from PM<sub>2.5</sub>, it is known that precursors are all primary pollutants. That is, the response of precursor concentration to the corresponding precursor emissions is linear (Cohan et al., 2005). Therefore, linear function between the concentration of each precursor and the total emissions of the corresponding precursor is fitted in region *r* deriving from the training samples for pf-ERSM development (Table S2) firstly.

$$\Delta\text{Conc}[P]_r = X_r \cdot E[P]_r \quad (3)$$

where  $P$  represents one precursor, i.e., NO<sub>x</sub>, SO<sub>2</sub> or NH<sub>3</sub>.  $\Delta\text{Conc}[P]_r$  is the concentration changes of precursor  $P$  in region *r* caused by the total emission changes of precursor  $P$  in region *r*.  $E[P]_r$  is the total emissions change ratio of precursor  $P$  in region *r*.  $X_r$  is the coefficient of region *r*.

Secondly, according to the concentration changes of precursor  $P$  in region *r* caused by emission changes of precursor  $P$  from different sectors in region *r* deriving from the training samples set in Table 1, the equivalent total emissions of precursor  $P$  of different sectors can be solved based on Eq. (4) converted from Eq. (3).

$$E[P]'_r = \Delta\text{Conc}[P]_{r-S_n} / X_r \quad (4)$$

where  $E[P]'_r$  is the change ratio of equivalent total emissions of precursor  $P$  in region *r*.  $\Delta\text{Conc}[P]_{r-S_n}$  is the concentration changes of precursor  $P$  in region *r* caused by the emission changes of precursor  $P$  from sector  $n$  in region *r*.

**Table 1**

Emissions control variables and scenarios selected for linear fitting of total precursor emissions to sectoral precursor emissions.

Control number	Control variable	Scenario number	Scenario details
7	7 variables in each of the 7 regions, i.e., (1) NO <sub>x</sub> /stationary combustion (2) NO <sub>x</sub> /on-road mobile (3) NO <sub>x</sub> /others (4) SO <sub>2</sub> /stationary combustion (5) SO <sub>2</sub> /others (6) NH <sub>3</sub> /agriculture (7) NH <sub>3</sub> /others	71	1 base case; 70 scenarios, 10 for each region, including 4 scenarios where one sectoral NO <sub>x</sub> is set to 0 for each of the first three scenarios and all sectoral NO <sub>x</sub> are set to 0 for the last scenario, 3 and 3 scenarios generated in the same way for SO <sub>2</sub> and NH <sub>3</sub> , respectively.

Then fit the linear function between the equivalent total emissions and sectoral emissions of precursor  $P$ .

$$E[P]_r' = \sum_{n=1}^m X_n \cdot E[P]_{r-S_n} \quad (5)$$

where  $E[P]_{r-S_n}$  is the change ratio of emissions of precursor  $P$  from sector  $n$  in region  $r$ .  $X_n$  is the coefficient of the sector  $n$ .

Thence, for one control scenario of sectoral precursor emissions, it will first be merged to a control scenario of total precursor emissions based on Eq. (5). Then the  $PM_{2.5}$  response can be obtained from pferSM using the merged control scenario as the input.

Moreover, the linear relationship between  $PM_{2.5}$  concentrations and primary  $PM_{2.5}$  emissions was integrated into the pf-ERSM-SL system as well to obtain the  $PM_{2.5}$  response to primary  $PM_{2.5}$  emissions from multiple regions and multiple sectors. The method to develop the relationship between  $PM_{2.5}$  concentrations and sectoral primary  $PM_{2.5}$  emissions is straightforward. Referring to the previous paper (Long et al., 2016), we predicted  $PM_{2.5}$  response owing to the sectoral primary  $PM_{2.5}$  emissions changes by simply interpolating between the base case and a control scenario, where one control variable of sectoral primary  $PM_{2.5}$  was 0 and the others stayed constant (Table S3).

### 2.3. Source contribution analysis method

#### 2.3.1. Brute force method

The traditional BFM, in which a number of sensitivity simulations are performed, each with one source eliminated or reduced and the differences between the results from the sensitivity and baseline simulations are attributed to the source eliminated or reduced (Burr and Zhang, 2011), is the simplest and easiest sensitivity analysis method (Yamaji et al., 2012). The advantage of BFM is that it can be applied to any model input parameters (e.g., emissions, initial condition, boundary condition and reaction rate) and the output is conceptually easy to explain and interpret (Itahashi et al., 2015). The inputs only involved emissions in this study.

The limitation that the computational burden grows rapidly with the number of input parameters in this approach is improved by RSM. When the response of  $PM_{2.5}$  to emissions of pollutants (i.e., primary  $PM_{2.5}$ ) is linear, the impact of all primary  $PM_{2.5}$  emission sources to  $PM_{2.5}$  is the simple addition of the impact of each primary  $PM_{2.5}$  emission source. Therefore, the contributions of primary  $PM_{2.5}$  emissions from multiple regions and sectors to  $PM_{2.5}$  can be apportioned by RSM with BFM accurately. However, if the response is nonlinear, i.e.,  $PM_{2.5}$  to precursor emissions, the direct combination of the impact of each precursor emission source is usually not equal to the impact of all precursor emission sources (Zhu et al., 2018). As a result, the contributions of precursor emissions from multiple regions and sectors to  $PM_{2.5}$  cannot be well quantified by BFM.

#### 2.3.2. Differential method

The interaction terms in the polynomial function for  $PM_{2.5}$  (Eq. (2)) represent the interactions (i.e., nonlinear effects) of precursor emissions to  $PM_{2.5}$ , which results in the deficiency of BFM. DM would be introduced to fill the gap. For convenience in the present discussion, take a

simple interaction term  $y = 2x_1x_2$  as an example. The actual total contribution should be 2 assuming that  $x_1$  and  $x_2$  were reduced from 1 to 0 simultaneously. Applying the BFM, i.e., let  $x_1$  and  $x_2$  decrease from 1 to 0 separately,  $x_1$  and  $x_2$  contributed 2 respectively. The accumulative contribution was 4 based on BFM, apparent inconsistency with the total contribution. Instead, DM dissected  $x_1$  and  $x_2$  changes into a series of small intervals (e.g.,  $k\Delta x_1$  and  $k\Delta x_2$ ); and then  $\Delta y$  for  $x_1$  was obtained when  $x_1$  changed  $\Delta x_1$  but  $x_2$  remained unchanged, next  $\Delta y$  for  $x_2$  was obtained when  $x_2$  changed  $\Delta x_2$  but  $x_1$  remained  $x_1 - \Delta x_1$ . Repeat the process until  $x_1$  and  $x_2$  were 0, as shown in Table 2. Then, the sum of  $\Delta y$  for  $x_1$  was the contribution of  $x_1$  and the sum of  $\Delta y$  for  $x_2$  was the contribution of  $x_2$ . The accumulative contribution of  $x_1$  and  $x_2$ , i.e., the sum of  $\Delta y$ , equalled to 2 based on DM, consistent with the actual total contribution.

Fig. 3a showed the diagram of DM and BFM based on the 2-D isopleths of  $PM_{2.5}$  concentration at Guangdongshangxueyuan at GZ to simultaneous changes of  $NO_x$  and  $NH_3$  emissions from GZ in October. Take the scenario where emissions of the two precursors were reduced by 100% as an example, in the process of the  $NO_x$  and  $NH_3$  emission ratios changing from (1,1) to (0,0), which was indicated by the black dotted line, the total contribution of  $NO_x$  and  $NH_3$  was the  $PM_{2.5}$  concentration difference between (1, 1) and (0, 0). To distinguish the contributions of  $NO_x$  and  $NH_3$ , BFM thought the  $PM_{2.5}$  changes from (1, 1) to (1,0), i.e., the horizontal black solid line, was the contribution of  $NO_x$  emissions and the  $PM_{2.5}$  changes from (1, 1) to (0,1), i.e., the vertical black solid line, was the contribution of  $NH_3$  emissions. While, DM defined the sum of  $PM_{2.5}$  changes along every red solid line and every blue solid line as the contributions of  $NO_x$  and  $NH_3$ , respectively. By subdividing the  $NO_x$  and  $NH_3$  emissions change, the DM had the ability to reproduce the nonlinear response surface of  $PM_{2.5}$ .

Theoretically, the more the differential intervals were, the more coincident the red and blue solid lines would be to the black dotted line. As a result, the accumulative contribution of DM can be closer to the total contribution. However, the more differential intervals would bring about more computing burden. As shown in Fig. 3b, with the increase in differential intervals, the computing time increased almost linearly. It was found that the contribution ratio of  $NO_x$  and  $NH_3$  converged to a specific value and it hardly changed when the value of differential intervals was  $>30$ . Meanwhile, this value of differential intervals (i.e., 30) was enough to make the accumulative contribution by DM equal to the total contribution, as shown in Fig. 3c. Moreover, this particular law would be also applicable to other cases (e.g., simultaneous changes in emissions of two precursors of other interaction terms, as shown in Fig. S2). Therefore, the value of differential intervals was determined as 30 eventually in this study.

The comparison of the case was shown in Fig. 3c. Based on BFM, the contributions of  $NO_x$  emissions and  $NH_3$  emissions were  $0.96 \mu g m^{-3}$  and  $2.19 \mu g m^{-3}$ , respectively. The essence of BFM was to consider the influence of one precursor (i.e.,  $NO_x$  or  $NH_3$ ) emissions change alone as the contribution of the precursor. Therefore, the contribution of one precursor analyzed by BFM actually derived from the scenario when the particular precursor emissions were controlled, while the others stayed the same as the base case. Actually, when  $NO_x$  emissions and  $NH_3$  emissions changed together, the

**Table 2**  
Calculation process of the DM for the simplified interaction term.

Intervals	$x_1$	$x_2$	$y = 2x_1x_2$	$\Delta y$
1	$1 - \Delta x_1$	1	$2(1 - \Delta x_1)x_2$	$2 - 2(1 - \Delta x_1)x_2$
	$1 - \Delta x_1$	$1 - \Delta x_2$	$2(1 - \Delta x_1)(1 - \Delta x_2)$	$2(1 - \Delta x_1)x_2 - 2(1 - \Delta x_1)(1 - \Delta x_2)$
2	$1 - 2\Delta x_1$	$1 - \Delta x_2$	$2(1 - 2\Delta x_1)(1 - \Delta x_2)$	$2(1 - \Delta x_1)(1 - \Delta x_2) - 2(1 - 2\Delta x_1)(1 - \Delta x_2)$
	$1 - 2\Delta x_1$	$1 - 2\Delta x_2$	$2(1 - 2\Delta x_1)(1 - 2\Delta x_2)$	$2(1 - 2\Delta x_1)(1 - \Delta x_2) - 2(1 - 2\Delta x_1)(1 - 2\Delta x_2)$
k	$1 - k\Delta x_1$	$1 - (k - 1)\Delta x_2$	$2(1 - k\Delta x_1)(1 - (k - 1)\Delta x_2)$	$2(1 - (k - 1)\Delta x_1)(1 - (k - 1)\Delta x_2) - 2(1 - k\Delta x_1)(1 - (k - 1)\Delta x_2)$
	$1 - k\Delta x_1$	$1 - k\Delta x_2$	$2(1 - k\Delta x_1)(1 - k\Delta x_2)$	$2(1 - k\Delta x_1)(1 - (k - 1)\Delta x_2) - 2(1 - k\Delta x_1)(1 - k\Delta x_2)$

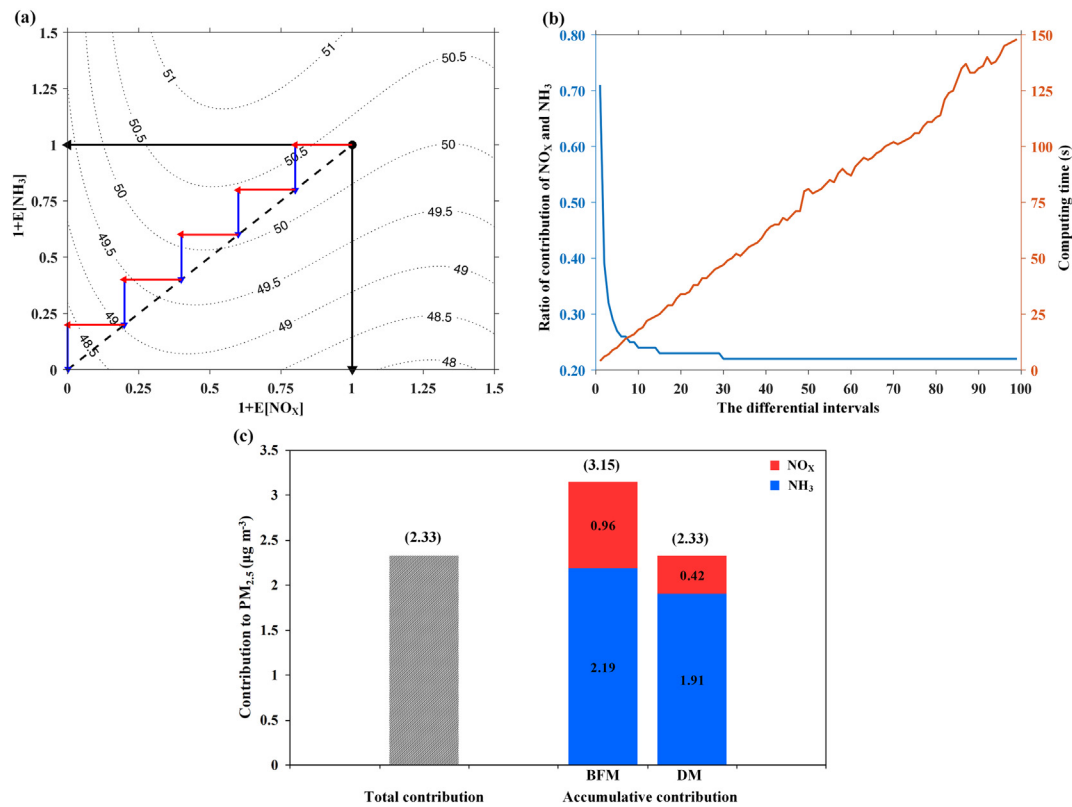


**Fig. 3.** (a) The diagram of DM and BFM based on the example case. The black solid lines represented the emissions change in BFM, the red and blue solid lines represented the emissions change in DM, and the black dotted line represented the actual emissions change. (b) The trend of the ratio of contribution of NO<sub>x</sub> and NH<sub>3</sub> and the trend of computing time with the differential intervals for the case. (c) The comparison of the total contribution and the accumulative contribution solved by BFM and DM for the case. (For interpretation of the references to colour in this figure legend, the reader is referred to the web version of this article.)

total influence was often smaller than the sum of the two single effects, which mainly attributed to the overlapping effect of two precursors involved in the formation of ammonium sulfate (e.g., SO<sub>2</sub> and NH<sub>3</sub>) and ammonium nitrate (e.g., NO<sub>x</sub> and NH<sub>3</sub>) for PM<sub>2.5</sub>. It was evident that the accumulative contribution of BFM (3.15 μg m<sup>-3</sup>) was larger than the total contribution (2.33 μg m<sup>-3</sup>). For DM, when the value of differential intervals was 30, the contribution of NO<sub>x</sub> emissions was 0.42 μg m<sup>-3</sup>, and the contribution of NH<sub>3</sub> emissions was 1.91 μg m<sup>-3</sup>. The accumulative contribution by DM (i.e., 2.33 μg m<sup>-3</sup>) was the same as the total contribution.

### 3. Results and discussion

#### 3.1. Model performance

##### 3.1.1. Evaluation of WRF-CMAQ

The meteorological observation data at Shundesugang and Rongguijiedaoban were used to evaluate the performance of WRF model. Table S4 listed the statistical results of temperature, wind speed, and relative humidity for January, April, July, and October in 2015, respectively. As a whole, the performance of WRF was very acceptable. The simulation of wind speed was worse than temperature and relative humidity. The wind speed was biased high (Normalized Mean Bias, NMB: 101.02%) in January at Shundesugang. The correlation coefficients of temperature, wind speed, and relative humidity ranged from 0.73 to 0.93, from 0.48 to 0.78 and from 0.74 to 0.91, respectively. These values were within their typical range of meteorological modeling studies (Wang et al., 2016b; Yin et al., 2017).

Furthermore, the CMAQ model was evaluated. The time series plots of hourly simulated concentrations of PM<sub>2.5</sub> in January (Fig. S3), April

(Fig. S4), July (Fig. S5), and October (Fig. S6) in 2015 were compared with the observation data at 7 national controlled air quality monitoring sites in 7 regions for the base scenario. The statistic indicators, i.e., NMB and R, were summarized. Meanwhile, the scatter plots were shown in Fig. S7-S10. Temporal variations of PM<sub>2.5</sub> were well captured with correlation coefficients of 0.40 to 0.75. According to the recommended value of NMB (<±30%) (Emery et al., 2017), the simulated PM<sub>2.5</sub> showed satisfactory performance. These biases can be mainly attributed to the uncertainties in emissions, meteorological data, boundary condition, and chemical processes. The model performance statistics indicate that the WRF-CMAQ system is capable of simulating the major meteorological parameters and PM<sub>2.5</sub> concentration.

##### 3.1.2. Validation of pf-ERSM-SL

The reliability of the pf-ERSM-SL prediction system was tested by out-of-sample validation, i.e., comparing PM<sub>2.5</sub> concentrations predicted by pf-ERSM-SL with the corresponding CMAQ simulations for out-of-sample control scenarios. The 40 out-of-sample cases described in Table S5 were selected for validating the accuracy of predicting the PM<sub>2.5</sub> response to the emissions of precursors (case 1–10), primary PM<sub>2.5</sub> (case 11–15), precursor and primary PM<sub>2.5</sub> (case 16–30) and sectoral precursors (case 31–40), respectively. The performance of pf-ERSM-SL was evaluated based on five metrics, namely, mean square error (MSE), root mean squared error (RMSE), relative root mean squared error (RRMSE), average relative error (ARE), and correlation coefficient (CC, i.e., R). ARE was named by mean normalized error (MNE) in previous RSM researches for out-of-sample validation (Wang et al., 2011; Xing et al., 2018; Xing et al., 2011; Xing et al., 2017; Zhao et al., 2015; Zhao et al., 2017). The average and maximal

values (over out-of-sample cases) of these statistical indices were defined as follows:

$$aMSE = \frac{1}{K} \sum_{i=1}^K \left( \frac{1}{N} \sum_{i=1}^N (M_i - O_i)^2 \right) \tag{6}$$

$$\max MSE = \max \left( \sum_{i=1}^K \left( \frac{1}{N} \sum_{i=1}^N (M_i - O_i)^2 \right) \right) \tag{7}$$

$$aRMSE = \frac{1}{K} \sum_{i=1}^K \sqrt{\frac{1}{N} \sum_{i=1}^N (M_i - O_i)^2} \tag{8}$$

$$aRRMSE = \frac{1}{K} \sum_{i=1}^K \frac{\sqrt{\frac{1}{N} \sum_{i=1}^N (M_i - O_i)^2}}{\bar{M}} \tag{9}$$

$$aARE = \frac{1}{K} \sum_{i=1}^K \left( \frac{1}{N} \sum_{i=1}^N \frac{|M_i - O_i|}{O_i} \right) \tag{10}$$

$$\max ARE = \max \left( \sum_{i=1}^K \left( \frac{1}{N} \sum_{i=1}^N \frac{|M_i - O_i|}{O_i} \right) \right) \tag{11}$$

$$aCC = \frac{1}{K} \sum_{i=1}^K \frac{\sum_{i=1}^N (M_i - \bar{M})(O_i - \bar{O})}{\sqrt{\sum_{i=1}^N (M_i - \bar{M})^2 \sum_{i=1}^N (O_i - \bar{O})^2}} \tag{12}$$

where *K* refers to the number of out-of-sample cases. *N* is the number of grid cells. *M<sub>i</sub>* and *O<sub>i</sub>* are the pf-ERSM-SL-predicted and CMAQ-simulated value of the *i*th data in the series of grid cells. and are the average pf-ERSM-SL-predicted and CMAQ-simulated value over the series of grid cells.

Table 3 summarized the statistics for the comparison. It showed that the error of pf-ERSM-SL-predicted PM<sub>2.5</sub> was very low with aMSE of 0.00–0.32 μg m<sup>-3</sup>, aRMSE of 0.04–0.55 μg m<sup>-3</sup> and aRRMSE of 0.20–2.46%. The maxMSE was just 0.65 (case 37 of case 31–40 in October). Especially, the aAREs were lower than 2% and aCCs were >0.999 for 4 kinds of out-of-sample cases in 4 months. These values meet the criteria of the previous study (Xing et al., 2018), implying the PM<sub>2.5</sub> concentrations of pf-ERSM-SL-predicted and CMAQ-simulated were highly consistent. It can be seen that the maxAREs were within 0.38% and the aCCs were all almost 1 for case 11–15 in 4 months, indicating a perfect

linear relationship between PM<sub>2.5</sub> concentrations and primary PM<sub>2.5</sub> emissions. For case 31–40, the maxARE ranged from 0.66% in July to 2.30% in October. That is, the PM<sub>2.5</sub> response predicted by the pf-ERSM-SL system agreed well with the PM<sub>2.5</sub> concentration changes simulated by CMAQ due to sectoral precursor emissions changing, implying the indirect relationship of PM<sub>2.5</sub> response to sectoral precursor emissions developed in this study is reliable.

Additionally, Fig. 4 presented the spatial distribution of CMAQ-simulated and pf-ERSM-SL-predicted PM<sub>2.5</sub> concentration and their delta (pf-ERSM-SL minus CMAQ) for the case with the maximal ARE from out-of-sample case 31–40 in January, April, July, and October respectively. It can be seen that even in the scenario with the maximal MNE, the pf-ERSM-SL and CMAQ still made very similar predictions for PM<sub>2.5</sub> in the spatial patterns with the delta ranging from -0.77 μg m<sup>-3</sup> to 3.79 μg m<sup>-3</sup>, -2.55 μg m<sup>-3</sup> to 3.01 μg m<sup>-3</sup>, -1.66 μg m<sup>-3</sup> to 2.82 μg m<sup>-3</sup>, -2.98 μg m<sup>-3</sup> to 3.46 μg m<sup>-3</sup> across the domain in January, April, July and October respectively.

### 3.2. Comparison of DM and BFM for accumulative contribution of precursor emissions to PM<sub>2.5</sub>

The total contribution and the accumulative contribution of precursor emissions to 4-month mean PM<sub>2.5</sub> solved by BFM and DM at 6 receptors were compared in the scenarios where precursor emissions from all regions were controlled by 0%, 25%, 50%, 75% and 100% (Fig. 5). The accumulative contribution of precursor emissions to PM<sub>2.5</sub> solved by BFM was higher than the total reduction of PM<sub>2.5</sub>, and that by DM was almost the same as the total one, which was found at all reduction ratios in all receptors. For 100% control of precursor emissions from all regions, the accumulative contribution to PM<sub>2.5</sub> calculated by BFM was overestimated by 1.76 μg m<sup>-3</sup> at SD, 1.54 μg m<sup>-3</sup> at FS, 1.57 μg m<sup>-3</sup> at GZ, 1.81 μg m<sup>-3</sup> at ZS, 2.00 μg m<sup>-3</sup> at JM, and 1.62 μg m<sup>-3</sup> at DG&SZ, about 32%, 20%, 29%, 22%, 20%, and 28% respectively. With the increase in reduction ratio of precursor emissions, the tendency of accumulative contribution apportioned by the DM completely matched the trend of total PM<sub>2.5</sub> reduction in all receptors. Note that the growth rate of accumulative contribution by BFM slightly decreased with the increase in reduction ratio, while that by DM gradually increased. It indicated that an additional air quality benefit could be achieved if more control measures were implemented, larger than that expected from linear extrapolation.

To further compare the difference of BFM and DM, the spatial distribution of the total contribution and the accumulative contribution of precursor emissions to 4-month mean PM<sub>2.5</sub> calculated by the two methods in the simultaneous 100% reduction of precursor emissions

**Table 3**  
Comparison of pf-ERSM-SL-predicted and CMAQ-simulated PM<sub>2.5</sub> concentrations for out-of-sample validation.

Month	Case	aMSE (μg m <sup>-3</sup> )	maxMSE (μg m <sup>-3</sup> )	aRMSE (μg m <sup>-3</sup> )	aRRMSE (%)	aARE (%)	maxARE (%)	aCC
January	Case 1–10	0.09	0.43	0.26	1.11	0.67	1.75	0.9998
	Case 11–15	0.00	0.02	0.05	0.22	0.09	0.36	1.0000
	Case 16–30	0.07	0.16	0.25	1.19	0.75	1.18	0.9997
	Case 31–40	0.17	0.35	0.40	1.76	0.98	1.56	0.9995
April	Case 1–10	0.04	0.16	0.20	0.96	0.64	1.37	0.9999
	Case 11–15	0.00	0.02	0.05	0.24	0.11	0.40	1.0000
	Case 16–30	0.07	0.19	0.25	1.36	0.92	1.98	0.9997
	Case 31–40	0.14	0.27	0.36	1.86	1.22	2.07	0.9995
July	Case 1–10	0.00	0.01	0.06	0.43	0.25	0.44	1.0000
	Case 11–15	0.00	0.00	0.05	0.40	0.09	0.22	1.0000
	Case 16–30	0.01	0.03	0.10	0.88	0.46	1.16	0.9998
	Case 31–40	0.02	0.02	0.12	0.95	0.41	0.66	0.9999
October	Case 1–10	0.09	0.36	0.27	1.16	0.66	1.39	0.9998
	Case 11–15	0.00	0.02	0.04	0.20	0.05	0.38	1.0000
	Case 16–30	0.16	0.37	0.38	1.79	1.04	2.19	0.9995
	Case 31–40	0.32	0.65	0.55	2.46	1.35	2.30	0.9992

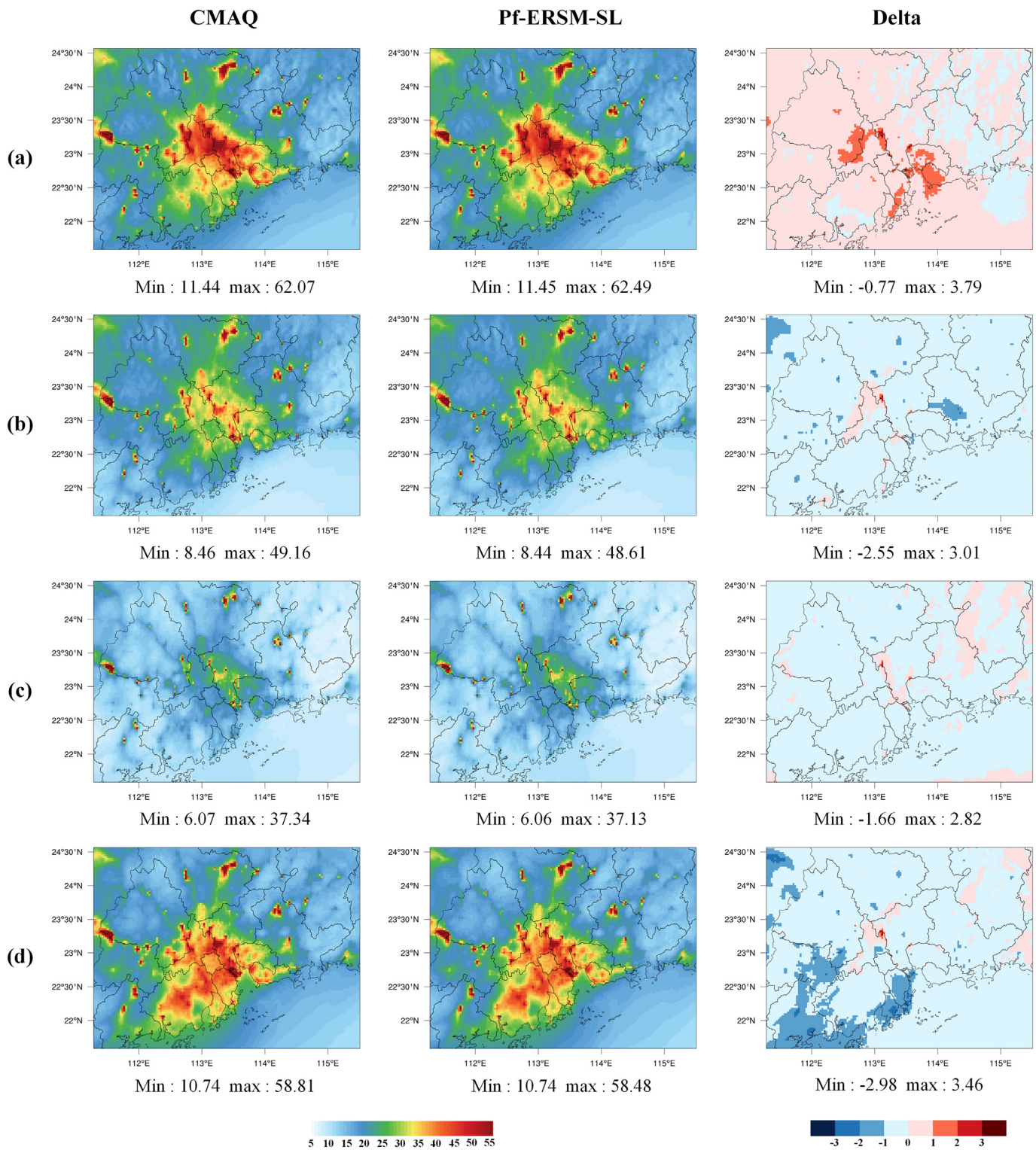


**Fig. 4.** Spatial distribution of CMAQ-simulated and pF-ERSM-SL-predicted PM<sub>2.5</sub> concentration and their delta (pF-ERSM-SL minus CMAQ) in the case with the maximal ARE from out-of-sample case 31–40 in (a) January, (b) April, (c) July, and (d) October (unit:  $\mu\text{g m}^{-3}$ ).

was shown in Fig. 6. Similar to the previous conclusion, the accumulative contribution calculated by the BFM was often higher than the total contribution for most grid cells, and that calculated by the DM was almost the same as the total contribution across the whole domain. The BFM overestimated approximately by  $1 \mu\text{g m}^{-3}$  to  $2 \mu\text{g m}^{-3}$  in the most grid cells and by  $2 \mu\text{g m}^{-3}$  to  $4 \mu\text{g m}^{-3}$  in the rest grid cells of 6

central regions (SD, FS, GZ, ZS, JM, DG&SZ). In perspective of the whole domain, the accumulative contributions of those grid cells with more precursor emissions, especially more NH<sub>3</sub> emissions (Fig. S11), were often overestimated more. Because the stronger the nonlinearity of PM<sub>2.5</sub> to precursor emissions was, the more the accumulative contribution calculated by the BFM would be overestimated in the grid cell.

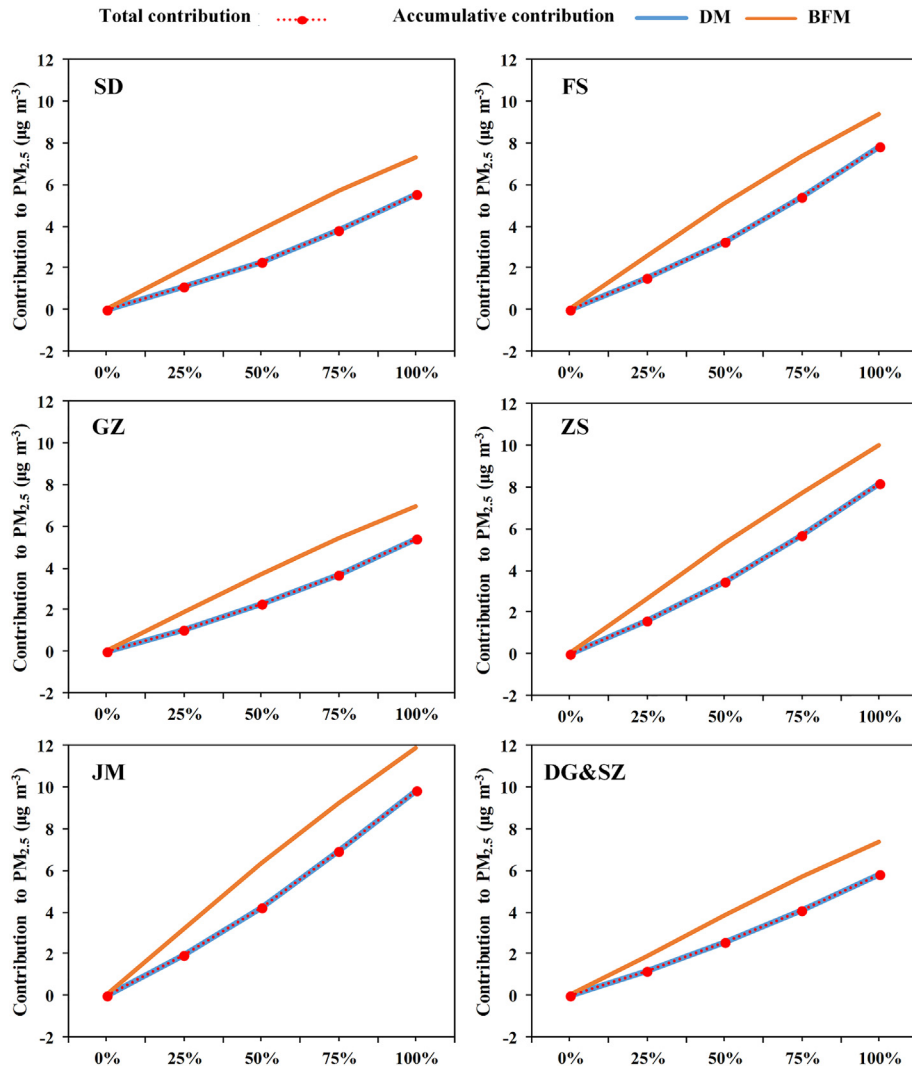


**Fig. 5.** Comparison between the total contribution and the accumulative contribution to 4-month mean  $PM_{2.5}$  solved by the BFM and the DM at 6 receptors in the scenarios where precursor emissions from all regions were reduced by 0%, 25%, 50%, 75%, and 100%. The x-axis showed the reduction ratio (i.e., 1-emission ratio).

### 3.3. Sensitivity analysis of $PM_{2.5}$

$PM_{2.5}$  sensitivity, which means the change ratio of  $PM_{2.5}$  concentration to the change ratio of each pollutant emissions, was quantified following previous studies (Wang et al., 2011; Zhao et al., 2015; Zhao et al., 2017).

$$S_a^X = [(C^* - C_a)/C^*]/(1-a) \quad (13)$$

where  $S_a^X$  is the  $PM_{2.5}$  sensitivity to pollutant X (i.e.,  $NO_x$ ,  $NH_3$ ,  $SO_2$ , VOC, and primary  $PM_{2.5}$ ) at its emission ratio a;  $C^*$  and  $C_a$  are  $PM_{2.5}$  concentrations in the base case (when the emission ratio of X is 1) and the control scenario (when the emission ratio of X is a), respectively.

Fig. 7 illustrated the 4-month mean and monthly mean  $PM_{2.5}$  sensitivities to the stepped control of individual pollutant emissions from all regions. Among all pollutants, the 4-month mean  $PM_{2.5}$  was the most sensitive to the emissions of primary  $PM_{2.5}$  in all 6 receptors. The  $PM_{2.5}$  sensitivities to primary  $PM_{2.5}$  emissions remained constant at various reduction ratios. Unlike primary  $PM_{2.5}$ , the  $PM_{2.5}$  sensitivities to precursors were different at various reduction ratios. Among the precursors,  $PM_{2.5}$  concentrations were primarily sensitive to the emissions of  $NH_3$  owing to the  $NH_3$ -poor regime in the PRD region. The  $PM_{2.5}$  sensitivities to the emissions of  $SO_2$  and VOC were small and changed

slightly with the increase in reduction ratio, mainly attributed to low emissions of  $SO_2$  (Xia et al., 2016) and underestimation of SOA in the CMAQ, which is also a common issue for most widely used chemical transport models (Robinson et al., 2007). However, the  $PM_{2.5}$  sensitivities to  $NO_x$  emissions increased significantly with the increase in reduction ratio. For instance,  $PM_{2.5}$  sensitivities in SD and GZ transferred from negative at low reduction ratios to positive at high reduction ratios. This strong nonlinearity had also been confirmed by the previous studies (Cai et al., 2017; Dong et al., 2014; Zhao et al., 2013; Zhao et al., 2015; Zhao et al., 2017).

$PM_{2.5}$  sensitivities to primary  $PM_{2.5}$  emissions were approximately the same in different months. However, there were some differences in  $PM_{2.5}$  sensitivities to emissions of precursors. In January,  $PM_{2.5}$  was the most sensitive to  $NH_3$ , followed by VOC. In April, July and October, the relative contributions of  $NO_x$ ,  $SO_2$ , and  $NH_3$  differed at various reduction ratios; and  $PM_{2.5}$  showed relatively less sensitive to VOC than in January. In October,  $PM_{2.5}$  was more sensitive to VOC emissions than in April and July and more sensitive to  $SO_2$  emissions than in January. This was mainly related to the formation mechanism of  $PM_{2.5}$  components under different meteorological conditions. For example, dry air and low temperature in January do not benefit to  $SO_2$  aqueous oxidation, i.e., the formation of sulfate. It was noteworthy that even a very large reduction ratio (75%) would lead to an increase for  $PM_{2.5}$  concentrations at SD, FS, and GZ in January if only  $NO_x$  emissions within the

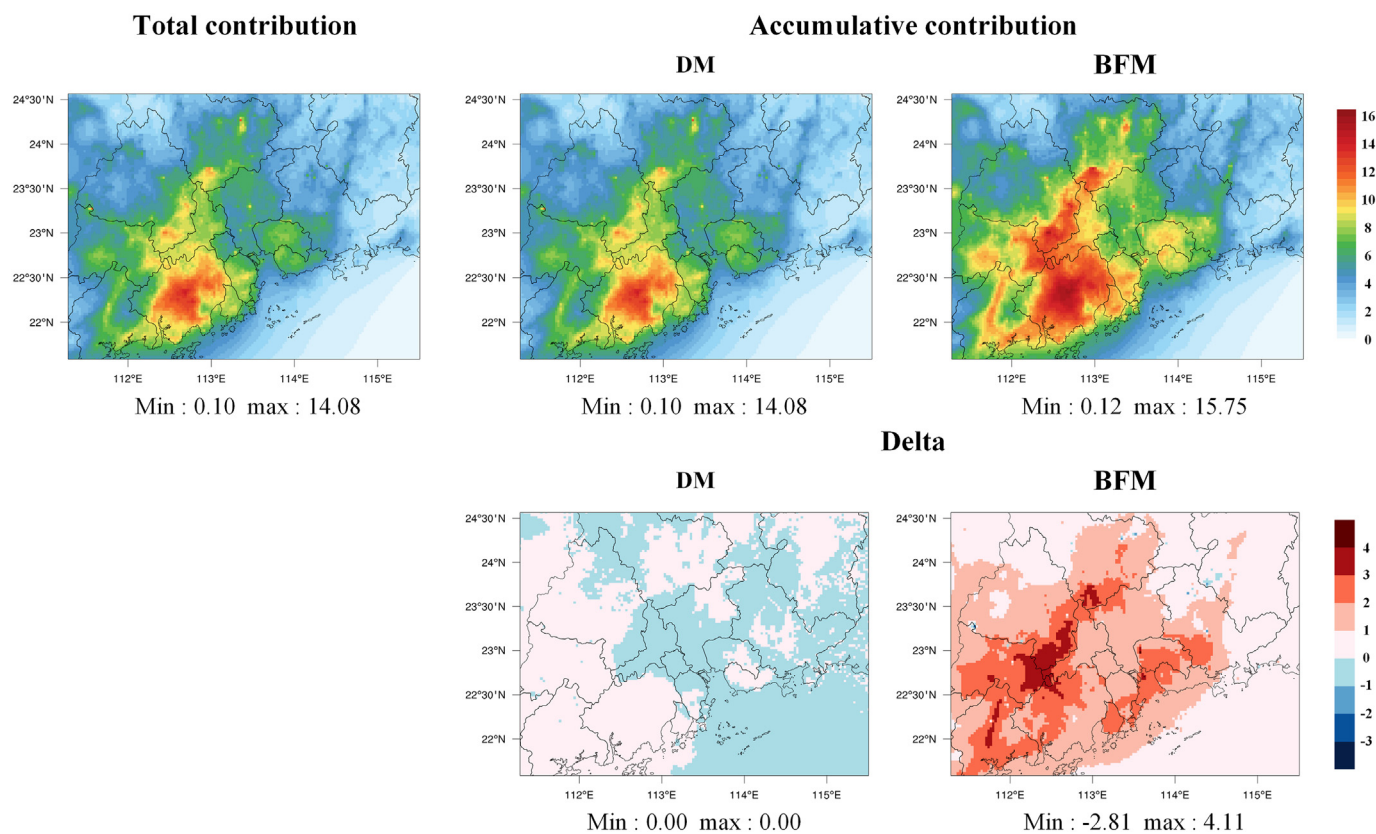


**Fig. 6.** Spatial distribution of the total contribution and the accumulative contribution of precursor emissions to 4-month mean  $PM_{2.5}$  solved by BFM and DM in the simultaneous 100% reduction of precursor emissions (unit:  $\mu g m^{-3}$ ).

PRD region were controlled, as a result of a strong VOC-limited regime. To achieve  $PM_{2.5}$  reduction in January with the prevailing northeasterly wind, it would be necessary to simultaneously reduce  $NO_x$  emissions from northern and eastern mainland of China outside the PRD region. This is because  $NO_x$  emission reductions in upwind regions are more likely to result in a net  $PM_{2.5}$  decrease compared with local emission reductions since the photochemistry typically changes from a VOC-limited regime in local urban areas at the surface to a  $NO_x$ -limited regime in downwind areas or at upper levels (Xing et al., 2011). Therefore there existed a phenomenon (shown in Fig. 7b) that the  $NO_x$  emission reductions can lead to  $PM_{2.5}$  decrease in downwind regions (ZS, JM, DG&SZ) in January. In July,  $NO_x$  emission reductions always induced a decrease in  $PM_{2.5}$  due to an  $NO_x$ -limited photochemical regime. The contribution of  $SO_2$  emissions to  $PM_{2.5}$  sensitivities was larger than that of  $NH_3$  and  $NO_x$  at small reductions. With the increase in reduction ratio, the contributions of  $SO_2$ ,  $NO_x$ , and  $NH_3$  became closer.

### 3.4. Source contribution analysis of $PM_{2.5}$

Employing DM and BFM for apportioning emission sources of precursors and primary  $PM_{2.5}$  respectively, we studied the emission contributions of multiple pollutants from different regions and different sectors to  $PM_{2.5}$  concentrations predicted by pf-ERSM-SL at receptors in the control scenario where all pollutant emissions reduced by 100%. In the process, we assumed that the contribution of precursor emissions from each source region to the changes of  $PM_{2.5}$  at receptors caused by IR can be estimated by its contribution to that caused by SR. After the DM apportioning the contribution of each precursor, the contribution of each sector of one precursor was obtained through the coefficient weight deriving from the relationship between total precursor emissions and sectoral ones (Eq. (5)).

Fig. 8 showed the contributions of pollutant emissions from different regions and different sectors (7 source regions  $\times$  12 source sectors = 84

source categories in total) to 4-month mean  $PM_{2.5}$  at 6 receptors. Table S6 listed the corresponding values. In the 100% control scenario, the anthropogenic emissions contributed  $24.21 \mu g m^{-3}$ ,  $27.66 \mu g m^{-3}$ ,  $28.26 \mu g m^{-3}$ ,  $25.91 \mu g m^{-3}$ ,  $25.70 \mu g m^{-3}$ ,  $20.42 \mu g m^{-3}$  accumulatively to 4-month mean  $PM_{2.5}$  at SD, FS, GZ, ZS, JM, DG&SZ, respectively. First, the contributions of pollutant emissions from different regions (7 source regions) to 4-month mean  $PM_{2.5}$  at 6 receptors were analyzed. The contributions of local emissions (i.e., emissions from the receptor) at GZ and DG&SZ,  $17.52 \mu g m^{-3}$  (62%) and  $13.15 \mu g m^{-3}$  (64%) respectively, were larger than that of regional emissions (i.e., emissions from other 6 regions except the receptor),  $10.74 \mu g m^{-3}$  (38%) and  $6.27 \mu g m^{-3}$  (36%) respectively. This was mainly caused by the high emissions intensity in local. However, local emissions contributed less than regional ones at other receptors (SD, FS, ZS, JM). Among them, SD was least affected by local emissions and most affected by regional emissions; and they contributed  $4.08 \mu g m^{-3}$  (17%) and  $20.13 \mu g m^{-3}$  (83%), respectively. This is because SD located in the center of the study domain with small areas. Generally, single-regional emissions (0–29%), i.e., emissions from one of the other 6 regions, contributed less than local emissions (39–64%) to 4-month mean  $PM_{2.5}$  at most receptors (FS, GZ, ZS, JM, DG&SZ); but emissions from GZ (33%) contributed more than local emissions (17%) at SD.

Secondly, the contributions of pollutant emissions from different sectors (12 source sectors) to 4-month mean  $PM_{2.5}$  at 6 receptors were discussed. It can be known that 4-month mean  $PM_{2.5}$  at 6 receptors were contributed most by primary  $PM_{2.5}$  emissions (62–81%). Among emissions of 4 precursors, the contributions of  $NH_3$  (9–18%) were larger than that of other precursors ( $NO_x$ , 2–12%;  $SO_2$ , 5–6%; VOC, 3–4%). Decomposed into various sectors, the primary  $PM_{2.5}$  emissions from dust source (road dust and construction dust) were found to make the largest contributions (25–42%), followed by that from other sources, i.e., industrial process source, etc., contributing 14% to 29%. The primary  $PM_{2.5}$  from stationary combustion and on-road mobile

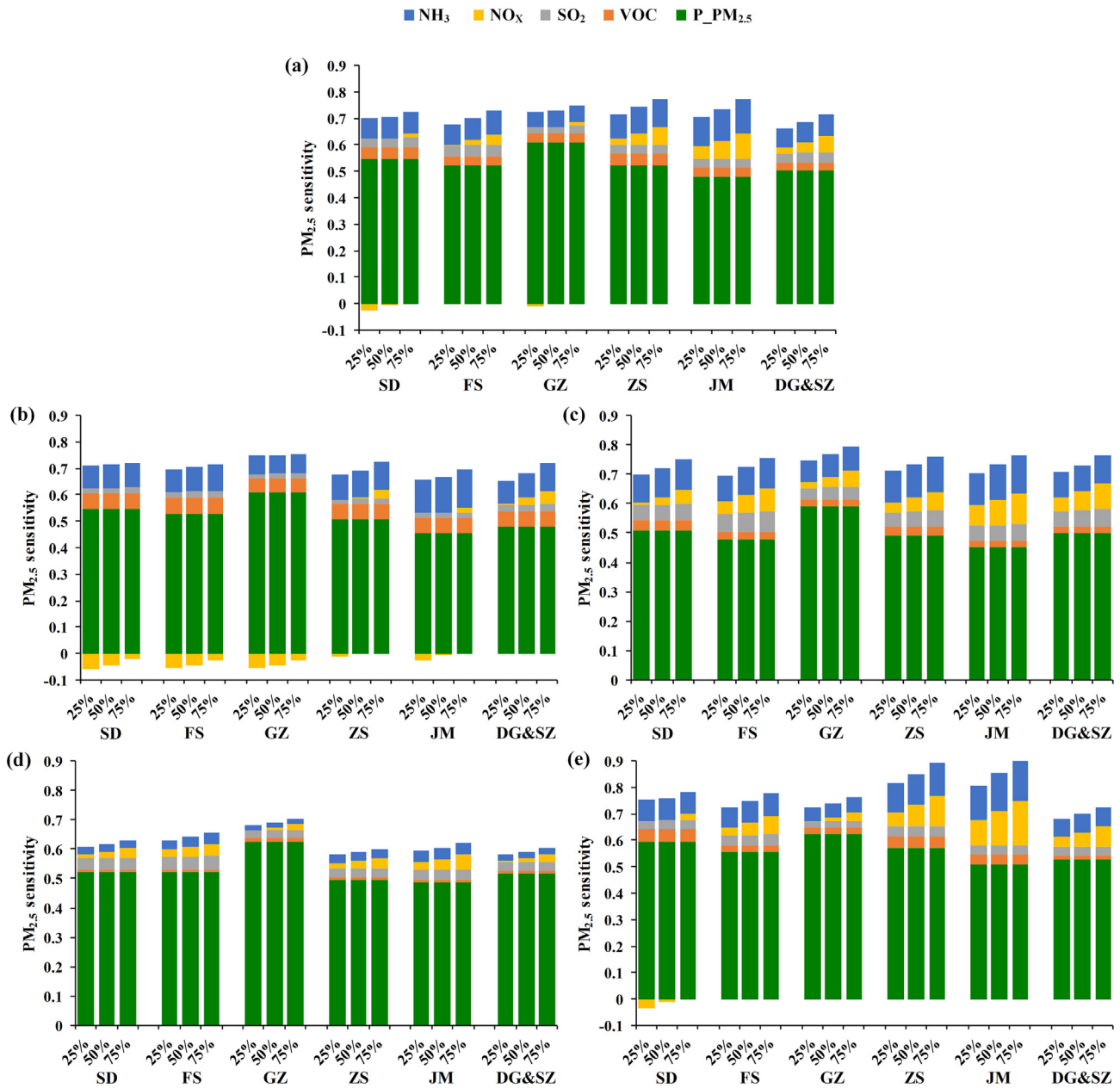


Fig. 7. PM<sub>2.5</sub> sensitivities of (a) 4-month mean, (b) January, (c) April, (d) July, and (e) October to the stepped control of individual pollutant emissions from all regions. The x-axis showed the reduction ratio (i.e., 1-emission ratio).

source contributed less than that from dust source and other sources. Among sub-sectors of precursor emissions, NH<sub>3</sub> emitted from agriculture source was generally the greatest contributor at most receptors (FS, GZ, ZS, JM), accounting for 6–13%; but NH<sub>3</sub> emitted from other sources, i.e., residential source, etc., also contributed a lot (SD, 6%) or even more than the former (DG&SZ, 9%). As for NO<sub>x</sub> emissions, the contributions of stationary combustion source were more than that of the other two sub-sectors, i.e., on-road mobile source and other sources. It was mainly the consequence that the adverse effects of NO<sub>x</sub> emissions from low-level sources owing to the reduction in consumption of ozone by the titration of NO (Deng et al., 2018). Then SO<sub>2</sub> emitted from stationary combustion source and other sources, i.e., non-road mobile source, etc., contributed almost the same. The results were explainable. During China's 11th Five-Year Plan (FYP) (2006–2010) and 12th FYP (2011–2015), the policies implemented to control on-road emissions (e.g., replacing yellow-label vehicles and improving the quality of diesel) and industrial emissions (e.g., the installation of flue-gas

desulfurization (FGD) equipment in the power sector and the implementation of new emission standards in key industrial sources) across the PRD region have been quite useful for reducing SO<sub>2</sub>, NO<sub>x</sub> and primary PM<sub>2.5</sub> emissions. Compared with on-road mobile source, emissions from the non-road mobile source were less regulated but it had been proved to be non-negligible. Although the related dust removal and FGD equipment were widely installed in factories, the increase in production output and the construction of new factories may offset the effects of control measures in the industrial process source (Lu et al., 2019). Additionally, the need for economic development has led to a dramatical increase in construction activities over the PRD region (Zhong et al., 2018). Moreover, it brought about more road dust that the total possession of vehicles has consistently increased over these 10 years. As is well known, NH<sub>3</sub> emissions are mainly from agriculture activities. NH<sub>3</sub> emissions have been regulated gradually in recent years due to its critical effects on PM<sub>2.5</sub>. For instance, 80.1% of collectible agricultural residue was used as fertilizer, feed, or transformed to clean

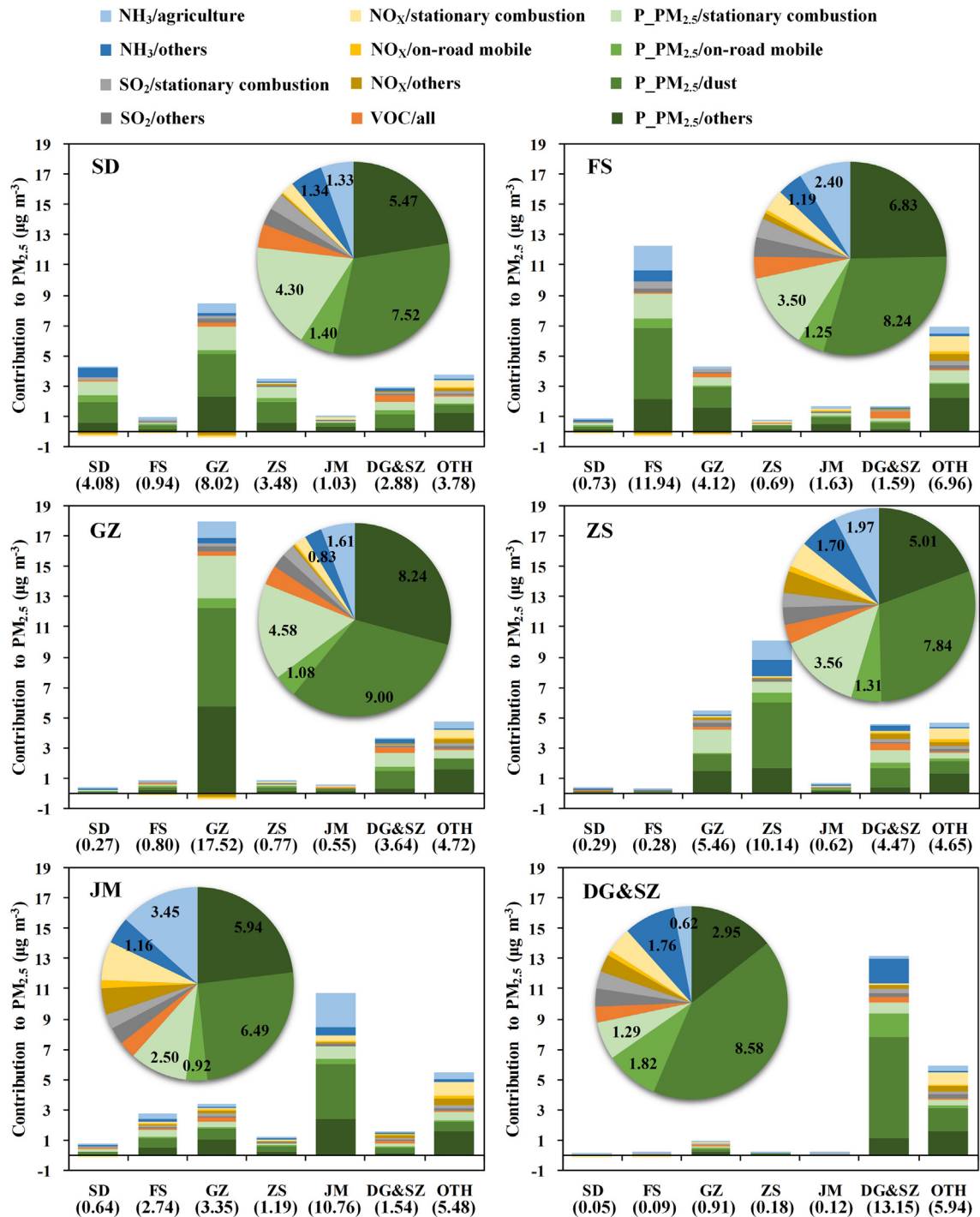


Fig. 8. Contributions of multiple pollutant emissions from different regions and different sectors to 4-month mean PM<sub>2.5</sub> concentrations at 6 receptors. The numbers in the pie chart showed the individual sector contributions. The numbers on the x-axis showed the individual region contributions.

energy in China in 2015 (Wang et al., 2017a). However, as the central and most developed region in Guangdong Province, the intensive human activities of the PRD region led to more NH<sub>3</sub> emissions from residential source, such as the human body and cooking sources.

Then the contributions of different pollutants from different regions and different sectors (84 source categories) to 4-month mean PM<sub>2.5</sub> were further analyzed at 6 receptors. The local primary PM<sub>2.5</sub> emissions from dust source were naturally the most significant contributor to 4-month mean PM<sub>2.5</sub> at most receptors (FS, GZ, ZS, JM, DG&SZ), accounting for 14% to 33% of the total contribution. The largest contributor to 4-

month mean PM<sub>2.5</sub> at SD was the primary PM<sub>2.5</sub> emissions of dust source from GZ, accounting for 11% of the total contribution. The contributions of NO<sub>x</sub> emissions from some regions (SD, FS, GZ) to 4-month mean PM<sub>2.5</sub> at some receptors (SD, FS, GZ, JM, DG&SZ) were negative, most of which was brought by low-level sources. There were some discrepancies between sectoral contributions of 6 major regions and that of OTH (including regions outside the PRD region) to receptors, such as fewer contributions of primary PM<sub>2.5</sub> from dust source and more contributions of NH<sub>3</sub> from agriculture source, attributing to differences in economic development.

The seasonal features of source contributions were further studied. SD, located in the center of the study domain (Fig. 2b), was chosen as an example. The results were shown in Fig. 9 and the corresponding values were listed in Table S7. The accumulative contributions of all emissions to PM<sub>2.5</sub> at SD were 28.30 μg m<sup>-3</sup>, 23.31 μg m<sup>-3</sup>, 13.03 μg m<sup>-3</sup>, 32.21 μg m<sup>-3</sup> in January, April, July, and October respectively. This was mainly related to the monthly mean PM<sub>2.5</sub> concentrations in the base case. The PM<sub>2.5</sub> concentration level in July was the lowest in 4 months, mainly because the weather conditions in summer benefit to the dilution of pollutants. In contrast, meteorological conditions, such as poor dispersion in fall and winter, are often not conducive to the removal of pollutants, attributing to high PM<sub>2.5</sub> concentration levels in October and January. However, spring is often a transmission season. Hence, the PM<sub>2.5</sub> concentration level in April was higher than that in July but lower than that in October and January.

Weather condition was the main factor deciding the relative contributions of different regions to PM<sub>2.5</sub> at SD in different months. In January and October, the contributions of pollutant emissions from GZ were much larger than those from other regions. This is because the dominant wind is northeasterly in October and January, so the polluted air-mass from GZ is blown down. In contrast, the prevailing southeasterly wind in July brings air-mass from ZS; thus, the pollutant emissions from ZS are the biggest contributor in July. However, the predominant wind direction can change in April. For example, the wind field changed from northeasterly in early spring to southwesterly in late spring (Lu et al., 2009). Therefore, the contributions of pollutant emissions from JM and ZS became a little larger, and that from GZ became a little smaller. As for the contributions of different sectors to PM<sub>2.5</sub> in different months, the characteristic was approximately consistent with that to the 4-month mean PM<sub>2.5</sub> at SD.

#### 4. Conclusions, implications, and limitations

In this study, the innovative pf-ERSM-SL with DM and BFM was developed. The pf-ERSM-SL predictions showed good agreement with the CMAQ simulations, and the DM was proved to be able to well address the issue of BFM in overestimating the accumulative contribution of precursor emissions to PM<sub>2.5</sub>.

Take the PRD region as a case, the sensitivities of PM<sub>2.5</sub> to pollutant emissions were first investigated. It was found that PM<sub>2.5</sub> was much more sensitive to the emissions of primary PM<sub>2.5</sub> than that of precursors. Among the precursors, PM<sub>2.5</sub> was mainly sensitive to NH<sub>3</sub> emissions. With the increase in reduction ratio, the sensitivities of PM<sub>2.5</sub> to NO<sub>x</sub> emissions increased substantially. Furthermore, the emission contributions of multiple pollutants from different sectors and multiple regions to PM<sub>2.5</sub> in the PRD region were quantified. The results demonstrated that PM<sub>2.5</sub> was generally dominated by local emission sources (39–64%). Among all pollutants, primary PM<sub>2.5</sub> made the largest contribution (62–81%) to PM<sub>2.5</sub>. The contributions of NH<sub>3</sub> (9–18%) were larger than that of other precursors (NO<sub>x</sub>, 2–12%; SO<sub>2</sub>, 5–6%; VOC, 3–4%). For different pollutants from various sectors, the primary PM<sub>2.5</sub> emissions from dust source made the largest contribution (25–42%) to PM<sub>2.5</sub>. The NH<sub>3</sub> emitted from agriculture source was often the main contributor (6–13%) among sub-sectors of precursor emissions. As for NO<sub>x</sub> emissions, the contributions of stationary combustion source were more than that of the other two sectors. For different pollutants from various sectors and different regions, the local primary PM<sub>2.5</sub> emissions from dust source contributed most to PM<sub>2.5</sub>.

The source contribution analysis results can be used to support the PM<sub>2.5</sub> pollution control strategies in the PRD region. First, the local emissions control strategies are pretty necessary for PM<sub>2.5</sub> pollution

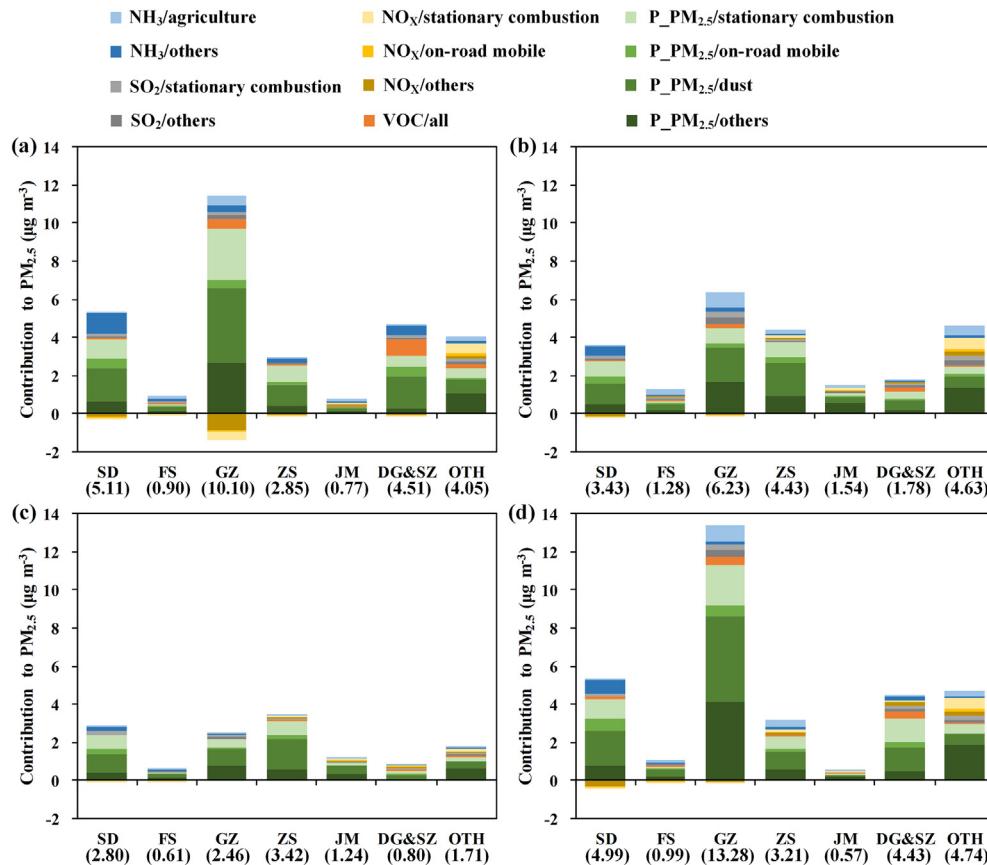


Fig. 9. Contributions of multiple pollutant emissions from different regions and different sectors to monthly mean PM<sub>2.5</sub> concentrations at SD in (a) January, (b) April, (c) July, and (d) October. The numbers on the x-axis showed the individual region contributions.

abatement. Second, the control of primary PM<sub>2.5</sub> emissions should be a priority in PM<sub>2.5</sub> control strategies. The primary PM<sub>2.5</sub> of dust source should be the focus since its contribution exceeded that of on-road mobile source and stationary combustion source. Third, the control of agriculture source should be included for the reason that it dominated the NH<sub>3</sub> emissions. Fourth, the control of NO<sub>x</sub> emitted from stationary combustion source should be more stringent. In addition to city-scale cooperation, joint control for province-to-province NO<sub>x</sub> emissions is also needed to further mitigate PM<sub>2.5</sub> pollution in the PRD region.

The pf-ERSM-SL with DM mainly provides an effective and efficient methodology for PM<sub>2.5</sub> source contribution analysis, thereby it is theoretically applicable to different geographical conditions. The application in other regions mainly limited by local emission inventory and meteorology, which will be taken into consideration in photochemical air quality models.

The pf-ERSM-SL with DM still has several limitations. First, the pf-ERSM-SL inherited uncertainties in the CMAQ simulations and emission inventory. Second, the pf-ERSM-SL currently was developed based on base-case meteorological conditions without consideration of the meteorological variability. Third, the application of pf-ERSM-SL with DM might be limited by computational resource consumption derived from hundreds of simulations.

### CRedit authorship contribution statement

**Yuzhou Pan:** Writing - original draft, Writing - review & editing, Methodology, Visualization, Validation. **Yun Zhu:** Conceptualization, Writing - review & editing, Software, Supervision. **Jicheng Jang:** Writing - review & editing, Supervision, Project administration. **Shuxiao Wang:** Data curation, Resources. **Jia Xing:** Software, Resources. **Pen-Chi Chiang:** Investigation, Formal analysis. **Xuetao Zhao:** Resources, Funding acquisition. **Zhiqiang You:** Formal analysis, Writing - review & editing. **Yingzhi Yuan:** Formal analysis.

### Declaration of competing interest

The authors declare that they have no known competing financial interests or personal relationships that could have appeared to influence the work reported in this paper.

### Acknowledgements

This work was supported by the Science and Technology Program of Guangzhou, China (No. 202002030188), the National Key Research and Development Program of China (No. 2016YFC0207605 and 2016YFC0207606), U.S. EPA Emission, Air quality, and Meteorological Modeling Support (No. EP-D-12-044), the National Natural Science Foundation of China (No. 21625701), the Fundamental Research Funds for the Central Universities (No. D2160320, D6180330, and D2170150) and the Natural Science Foundation of Guangdong Province, China (No. 2017A030310279).

### Appendix A. Supplementary data

Supplementary data to this article can be found online at <https://doi.org/10.1016/j.scitotenv.2020.139655>.

### References

- Bi, X.H., Feng, Y.C., Zhu, T., Zhang, Y.F., Wu, J.H., Li, X.A., 2011. Determination of buffering capacity of total suspended particle and its source apportionment using the chemical mass balance approach. *J. Air Waste Manage. Assoc.* 61, 7–13. <https://doi.org/10.3155/1047-3289.61.1.7>.
- Burr, M.J., Zhang, Y., 2011. Source apportionment of fine particulate matter over the eastern U.S. part I: source sensitivity simulations using CMAQ with the brute force method. *Atmos Pollut Res* 2, 300–317. <https://doi.org/10.5094/Apr.2011.036>.
- Cai, S.Y., Wang, Y.J., Zhao, B., Wang, S.X., Chang, X., Hao, J.M., 2017. The impact of the “air pollution prevention and control action plan” on PM<sub>2.5</sub> concentrations in Jing-Jin-Ji region during 2012–2020. *Sci. Total Environ.* 580, 197–209. <https://doi.org/10.1016/j.scitotenv.2016.11.188>.
- Chang, X., Wang, S., Zhao, B., Xing, J., Liu, X., Wei, L., Song, Y., Wu, W., Cai, S., Zheng, H., Ding, D., Zheng, M., 2019. Contributions of inter-city and regional transport to PM<sub>2.5</sub> concentrations in the Beijing-Tianjin-Hebei region and its implications on regional joint air pollution control. *Sci. Total Environ.* 660, 1191–1200. <https://doi.org/10.1016/j.scitotenv.2018.12.474>.
- Chen, D., Liu, X., Lang, J., Zhou, Y., Wei, L., Wang, X., Guo, X., 2017. Estimating the contribution of regional transport to PM<sub>2.5</sub> air pollution in a rural area on the North China Plain. *Sci. Total Environ.* 583, 280–291. <https://doi.org/10.1016/j.scitotenv.2017.01.066>.
- Chen, D.S., Zhao, N., Lang, J.L., Zhou, Y., Wang, X.T., Li, Y., Zhao, Y.H., Guo, X.R., 2018. Contribution of ship emissions to the concentration of PM<sub>2.5</sub>: a comprehensive study using AIS data and WRF/Chemmodel in Bohai rim region, China. *Sci. Total Environ.* 610, 1476–1486. <https://doi.org/10.1016/j.scitotenv.2017.07.255>.
- Cohan, D.S., Hakami, A., Hu, Y.T., Russell, A.G., 2005. Nonlinear response of ozone to emissions: source apportionment and sensitivity analysis. *Environ Sci Technol* 39, 6739–6748. <https://doi.org/10.1021/es048664m>.
- Deng, T., Huang, Y.Q., Li, Z.N., Wang, N., Wang, S.Q., Zou, Y., Yin, C.Q., Fan, S.J., 2018. Numerical simulations for the sources apportionment and control strategies of PM<sub>2.5</sub> over Pearl River Delta, China, part II: vertical distribution and emission reduction strategies. *Sci. Total Environ.* 634, 1645–1656. <https://doi.org/10.1016/j.scitotenv.2018.04.209>.
- Dong, X.Y., Li, J., Fu, J.S., Gao, Y., Huang, K., Zhuang, G.S., 2014. Inorganic aerosols responses to emission changes in Yangtze River Delta, China. *Sci. Total Environ.* 481, 522–532. <https://doi.org/10.1016/j.scitotenv.2014.02.076>.
- Dunker, A., 1984. The decoupled direct method for calculating sensitivity coefficients in chemical kinetics. *J. Chem. Phys.* 81, 2385–2393. <https://doi.org/10.1063/1.447938>.
- Dunker, A.M., Yarwood, G., Ortman, J.P., Wilson, G.M., 2002. Comparison of source apportionment and source sensitivity of ozone in a three-dimensional air quality model. *Environ Sci Technol* 36, 2953–2964. <https://doi.org/10.1021/es011418f>.
- Emery, C., Liu, Z., Russell, A.G., Odman, M.T., Yarwood, G., Kumar, N., 2017. Recommendations on statistics and benchmarks to assess photochemical model performance. *J. Air Waste Manage. Assoc.* 67, 582–598. <https://doi.org/10.1080/10962247.2016.1265027>.
- Fang, T., Zhu, Y., Jang, J., Wang, S., Xing, J., Chiang, P.-C., Fan, S., You, Z., Li, J., 2020. Real-time source contribution analysis of ambient ozone using an enhanced meta-modeling approach over the Pearl River Delta Region of China. *J. Environ. Manag.* 268, 110650. <https://doi.org/10.1016/j.jenvman.2020.110650>.
- GDEEP, 2016. 2015 report on the state of Guangdong provincial environment. [http://gdee.gd.gov.cn/hjzkgb/content/post\\_2335528.html](http://gdee.gd.gov.cn/hjzkgb/content/post_2335528.html), Accessed date: 18 December 2019.
- GDEEP, 2017. 2016 report on the state of Guangdong provincial environment. [http://gdee.gd.gov.cn/jg5875/content/post\\_2287908.html](http://gdee.gd.gov.cn/jg5875/content/post_2287908.html), Accessed date: 18 December 2019.
- GDEEP, 2018. 2017 report on the state of Guangdong provincial environment. [http://gdee.gd.gov.cn/hjzkgb/content/post\\_2335530.html](http://gdee.gd.gov.cn/hjzkgb/content/post_2335530.html), Accessed date: 18 December 2019.
- GDEEP, 2019. 2018 report on the state of Guangdong provincial environment. [http://gdee.gd.gov.cn/hjzkgb/content/post\\_2466184.html](http://gdee.gd.gov.cn/hjzkgb/content/post_2466184.html), Accessed date: 18 December 2019.
- Guenther, A., Karl, T., Harley, P., Wiedinmyer, C., Palmer, P.I., Geron, C., 2006. Estimates of global terrestrial isoprene emissions using MEGAN (Model of Emissions of Gases and Aerosols from Nature). *Atmos. Chem. Phys.* 6, 3181–3210. <https://doi.org/10.5194/acp-6-3181-2006>.
- Hakami, A., Odman, M.T., Russell, A.G., 2003. High-order, direct sensitivity analysis of multidimensional air quality models. *Environ Sci Technol* 37, 2442–2452. <https://doi.org/10.1021/es020677h>.
- Hakami, A., Odman, M.T., Russell, A.G., 2004. Nonlinearity in atmospheric response: a direct sensitivity analysis approach. *J. Geophys. Res.-Atmos.* 109. <https://doi.org/10.1029/2003jd004502>.
- Itahashi, S., Hayami, H., Uno, I., 2015. Comprehensive study of emission source contributions for tropospheric ozone formation over East Asia. *J. Geophys. Res.-Atmos.* 120, 331–358. <https://doi.org/10.1002/2014jd022117>.
- Ivey, C.E., Holmes, H.A., Hu, Y.T., Mulholland, J.A., Russell, A.G., 2015. Development of PM<sub>2.5</sub> source impact spatial fields using a hybrid source apportionment air quality model. *Geosci. Model Dev.* 8, 2153–2165. <https://doi.org/10.5194/gmd-8-2153-2015>.
- Kim, B.U., Bae, C., Kim, H.C., Kim, E., Kim, S., 2017. Spatially and chemically resolved source apportionment study of high particulate matter event. *Atmos. Environ.* 162, 55–70. <https://doi.org/10.1016/j.atmosenv.2017.05.006>.
- Koo, B., Wilson, G.M., Morris, R.E., Dunker, A.M., Yarwood, G., 2009. Comparison of source apportionment and sensitivity analysis in a particulate matter air quality model. *Environ Sci Technol* 43, 6669–6675. <https://doi.org/10.1021/es9008129>.
- Li, L., An, J.Y., Zhou, M., Qiao, L.P., Zhu, S.H., Yang, R.S., Ooi, C.G., Wang, H.L., Huang, C., Huang, L., Tao, S.K., Yu, J.Z., Chan, A., Wang, Y.J., Feng, J.L., Chen, C.H., 2018. An integrated source apportionment methodology and its application over the Yangtze River Delta Region, China. *Environ Sci Technol* 52, 14216–14227. <https://doi.org/10.1021/acs.est.8b01211>.
- Li, X., Zhang, Q., Zhang, Y., Zheng, B., Wang, K., Chen, Y., Wallington, T.J., Han, W.J., Shen, W., Zhang, X.Y., He, K.B., 2015. Source contributions of urban PM<sub>2.5</sub> in the Beijing-Tianjin-Hebei region: changes between 2006 and 2013 and relative impacts of emissions and meteorology. *Atmos. Environ.* 123, 229–239. <https://doi.org/10.1016/j.atmosenv.2015.10.048>.

- Long, S.C., Zhu, Y., Jang, C., Lin, C.J., Wang, S.X., Zhao, B., Gao, J., Deng, S., Xie, J.P., Qiu, X.Z., 2016. A case study of development and application of a streamlined control and response modeling system for PM<sub>2.5</sub> attainment assessment in China. *J Environ Sci-China* 41, 69–80. <https://doi.org/10.1016/j.jes.2015.05.019>.
- Lu, X., Chow, K.C., Yao, T., Fung, J.C.H., Lau, A.K.H., 2009. Seasonal variation of the land-sea breeze circulation in the Pearl River Delta region. *J. Geophys. Res.-Atmos.* 114. <https://doi.org/10.1029/2009jd011764>.
- Lu, X.C., Chen, Y., Huang, Y.Q., Lin, C.Q., Li, Z.Y., Fung, J.C.H., Lau, A.K.H., 2019. Differences in concentration and source apportionment of PM<sub>2.5</sub> between 2006 and 2015 over the PRD region in southern China. *Sci. Total Environ.* 673, 708–718. <https://doi.org/10.1016/j.scitotenv.2019.03.452>.
- Ma, Q.A., Cai, S.Y., Wang, S.X., Zhao, B., Martin, R.V., Brauer, M., Cohen, A., Jiang, J.K., Zhou, W., Hao, J.M., Frostad, J., Forouzanfar, M.H., Burnett, R.T., 2017. Impacts of coal burning on ambient PM<sub>2.5</sub> pollution in China. *Atmos. Chem. Phys.* 17, 4477–4491. <https://doi.org/10.5194/acp-17-4477-2017>.
- Napelenok, S.L., Vedantham, R., Bhavne, P.V., Pouliot, G.A., Kwok, R.H.F., 2014. Source-receptor reconciliation of fine-particulate emissions from residential wood combustion in the southeastern United States. *Atmos. Environ.* 98, 454–460. <https://doi.org/10.1016/j.atmosenv.2014.09.021>.
- Paatero, P., Tapper, U., 1994. Positive matrix factorization: a non-negative factor model with optimal utilization of error estimates of data values. *Environmetrics* 5, 111–126. <https://doi.org/10.1002/env.3170050203>.
- Robinson, A.L., Donahue, N.M., Shrivastava, M.K., Weitkamp, E.A., Sage, A.M., Grieshop, A.P., Lane, T.E., Pierce, J.R., Pandis, S.N., 2007. Rethinking organic aerosols: Semivolatile emissions and photochemical aging. *Science* 315, 1259–1262. <https://doi.org/10.1126/science.1133061>.
- Wang, G., Cheng, S.Y., Wei, W., Zhou, Y., Yao, S., Zhang, H.Y., 2016a. Characteristics and source apportionment of VOCs in the suburban area of Beijing, China. *Atmos Pollut Res* 7, 711–724. <https://doi.org/10.1016/j.apr.2016.03.006>.
- Wang, J.D., Zhao, B., Wang, S.X., Yang, F.M., Xing, J., Morawska, L., Ding, A.J., Kulmala, M., Kerminen, V.M., Kujansuu, J., Wang, Z.F., Ding, D.A., Zhang, X.Y., Wang, H.B., Tian, M., Petaja, T., Jiang, J.K., Hao, J.M., 2017a. Particulate matter pollution over China and the effects of control policies. *Sci. Total Environ.* 584, 426–447. <https://doi.org/10.1016/j.scitotenv.2017.01.027>.
- Wang, N., Lyu, X.P., Deng, X.J., Guo, H., Deng, T., Li, Y., Yin, C.Q., Li, F., Wang, S.Q., 2016b. Assessment of regional air quality resulting from emission control in the Pearl River Delta region, southern China. *Sci. Total Environ.* 573, 1554–1565. <https://doi.org/10.1016/j.scitotenv.2016.09.013>.
- Wang, S.X., Xing, J., Jang, C.R., Zhu, Y., Fu, J.S., Hao, J.M., 2011. Impact assessment of Ammonia emissions on inorganic aerosols in East China using response surface modeling technique. *Environ Sci Technol* 45, 9293–9300. <https://doi.org/10.1021/es2022347>.
- Wang, X.F., Zhang, Y.P., Chen, H., Yang, X., Chen, J.M., Geng, F.H., 2009. Particulate nitrate formation in a highly polluted urban area: a case study by single-particle mass spectrometry in Shanghai. *Environ Sci Technol* 43, 3061–3066. <https://doi.org/10.1021/es8020155>.
- Wang, Y.J., Bao, S.W., Wang, S.X., Hu, Y.T., Shi, X., Wang, J.D., Zhao, B., Jiang, J.K., Zheng, M., Wu, M.H., Russell, A.G., Wang, Y.H., Hao, J.M., 2017b. Local and regional contributions to fine particulate matter in Beijing during heavy haze episodes. *Sci. Total Environ.* 580, 283–296. <https://doi.org/10.1016/j.scitotenv.2016.12.127>.
- Watson, J., Cooper, J., Huntzicker, J., 1984. The effective variance weighting for least squares calculations applied to the mass balance receptor model. *Atmos. Environ.* 18, 1347–1355. [https://doi.org/10.1016/0004-6981\(84\)90043-X](https://doi.org/10.1016/0004-6981(84)90043-X).
- Wen, W., Cheng, S.Y., Liu, L., Wang, G., Wang, X.Q., 2016. Source apportionment of PM<sub>2.5</sub> in Tangshan, China-hybrid approaches for primary and secondary species apportionment. *Front Env Sci Eng* 10. <https://doi.org/10.1007/s11783-016-0839-9>.
- Xia, Y.M., Zhao, Y., Nielsen, C.P., 2016. Benefits of of China's efforts in gaseous pollutant control indicated by the bottom-up emissions and satellite observations 2000–2014. *Atmos. Environ.* 136, 43–53. <https://doi.org/10.1016/j.atmosenv.2016.04.013>.
- Xie, M., Zhu, K.G., Wang, T.J., Feng, W., Gao, D., Li, M.M., Li, S., Zhuang, B.L., Han, Y., Chen, P.L., Liao, J.B., 2016. Changes in regional meteorology induced by anthropogenic heat and their impacts on air quality in South China. *Atmos. Chem. Phys.* 16, 15011–15031. <https://doi.org/10.5194/acp-16-15011-2016>.
- Xing, J., Wang, S.X., Jang, C., Zhu, Y., Hao, J.M., 2011. Nonlinear response of ozone to precursor emission changes in China: a modeling study using response surface methodology. *Atmos. Chem. Phys.* 11, 5027–5044. <https://doi.org/10.5194/acp-11-5027-2011>.
- Xing, J., Wang, S.X., Zhao, B., Wu, W.J., Ding, D.A., Jang, C., Zhu, Y., Chang, X., Wang, J.D., Zhang, F.F., Hao, J.M., 2017. Quantifying nonlinear multiregional contributions to ozone and fine particles using an updated response surface modeling technique. *Environ Sci Technol* 51, 11788–11798. <https://doi.org/10.1021/acs.est.7b01975>.
- Xing, J., Ding, D., Wang, S.X., Zhao, B., Jang, C., Wu, W.J., Zhang, F.F., Zhu, Y., Hao, J.M., 2018. Quantification of the enhanced effectiveness of NO<sub>x</sub> control from simultaneous reductions of VOC and NH<sub>3</sub> for reducing air pollution in the Beijing-Tianjin-Hebei region, China. *Atmos. Chem. Phys.* 18, 7799–7814. <https://doi.org/10.5194/acp-18-7799-2018>.
- Yamaji, K., Uno, I., Irie, H., 2012. Investigating the response of East Asian ozone to Chinese emission changes using a linear approach. *Atmos. Environ.* 55, 475–482. <https://doi.org/10.1016/j.atmosenv.2012.03.009>.
- Yin, X.H., Huang, Z.J., Zheng, J.Y., Yuan, Z.B., Zhu, W.B., Huang, X.B., Chen, D.H., 2017. Source contributions to PM<sub>2.5</sub> in Guangdong province, China by numerical modeling: results and implications. *Atmos. Res.* 186, 63–71. <https://doi.org/10.1016/j.atmosres.2016.11.007>.
- You, Z.Q., Zhu, Y., Jang, C., Wang, S.X., Gao, J., Lin, C.J., Li, M.H., Zhu, Z.H., Wei, H., Yang, W.W., 2017. Response surface modeling-based source contribution analysis and VOC emission control policy assessment in a typical ozone-polluted urban Shunde, China. *J Environ Sci-China* 51, 294–304. <https://doi.org/10.1016/j.jes.2016.05.034>.
- Zhang, Y.J., Cai, J., Wang, S.X., He, K.B., Zheng, M., 2017. Review of receptor-based source apportionment research of fine particulate matter and its challenges in China. *Sci. Total Environ.* 586, 917–929. <https://doi.org/10.1016/j.scitotenv.2017.02.071>.
- Zhao, B., Wang, S.X., Wang, J.D., Fu, J.S., Liu, T.H., Xu, J.Y., Fu, X., Hao, J.M., 2013. Impact of national NO<sub>x</sub> and SO<sub>2</sub> control policies on particulate matter pollution in China. *Atmos. Environ.* 77, 453–463. <https://doi.org/10.1016/j.atmosenv.2013.05.012>.
- Zhao, B., Wang, S.X., Xing, J., Fu, K., Fu, J.S., Jang, C., Zhu, Y., Dong, X.Y., Gao, Y., Wu, W.J., Wang, J.D., Hao, J.M., 2015. Assessing the nonlinear response of fine particles to precursor emissions: development and application of an extended response surface modeling technique v1.0. *Geosci. Model Dev.* 8, 115–128. <https://doi.org/10.5194/gmd-8-115-2015>.
- Zhao, B., Wu, W.J., Wang, S.X., Xing, J., Chang, X., Liou, K.N., Jiang, J.H., Gu, Y., Jang, C., Fu, J.S., Zhu, Y., Wang, J.D., Lin, Y., Hao, J.M., 2017. A modeling study of the nonlinear response of fine particles to air pollutant emissions in the Beijing-Tianjin-Hebei region. *Atmos. Chem. Phys.* 17, 12031–12050. <https://doi.org/10.5194/acp-17-12031-2017>.
- Zhong, Z.M., Zheng, J.Y., Zhu, M.N., Huang, Z.J., Zhang, Z.W., Jia, G.L., Wang, X.L., Bian, Y.H., Wang, Y.L., Li, N., 2018. Recent developments of anthropogenic air pollutant emission inventories in Guangdong province, China. *Sci. Total Environ.* 627, 1080–1092. <https://doi.org/10.1016/j.scitotenv.2018.01.268>.
- Zhu, Y.H., Huang, L., Li, J.Y., Ying, Q., Zhang, H.L., Liu, X.G., Liao, H., Li, N., Liu, Z.X., Mao, Y.H., Fang, H., Hu, J.L., 2018. Sources of particulate matter in China: insights from source apportionment studies published in 1987–2017. *Environ. Int.* 115, 343–357. <https://doi.org/10.1016/j.envint.2018.03.037>.